# Material parameters of $In_{1-x}Ga_xAs_yP_{1-y}$ and related binaries

Sadao Adachi

Citation: Journal of Applied Physics **53**, 8775 (1982); doi: 10.1063/1.330480
View online: https://doi.org/10.1063/1.330480
View Table of Contents: http://aip.scitation.org/toc/jap/53/12
Published by the American Institute of Physics

# Material parameters of $In_{1-x}Ga_xAs_yP_{1-y}$ and related binaries

Sadao Adachi
*Musashino Electrical Communication Laboratory, Nippon Telegraph and Telephone Public Corporation, Musashino-shi, Tokyo 180, Japan*

(Received 15 March 1982; accepted for publication 20 July 1982)

Various models for calculation of physical parameters in compound alloys are discussed and the results for $In_{1-x}Ga_xAs_yP_{1-y}$ quaternaries are presented. The model used is based on a linear interpolation scheme, and therefore necessitates known values of the parameters for the related binary and ternary alloys. The material parameters considered in the present study can be classified into the following eleven groups: (1) lattice constant and crystal density, (2) thermal expansion coefficient, (3) electronic-band structure, (4) external perturbation effect on the lowest-direct gap, (5) effective mass, (6) dielectric constant, (7) Fröhlich coupling parameter, (8) elastic properties, (9) piezoelectric properties, (10) deformation potential, and (11) excitonic effect. Of particular interest is the deviation of material parameters from linearity with respect to the alloy composition. It is found that the present model provides generally acceptable parameters, in good agreement with the existing experimental data. A detailed discussion is also given on the acceptability of such interpolated parameters from an aspect of the solid-state physics. Key properties of the material parameters for a variety of $In_{1-x}Ga_xAs_yP_{1-y}$ device applications are also discussed.

PACS numbers: 71.25. – s, 72.20. – i, 77.60. + v, 78.20.Dj

## I. INTRODUCTION

$In_{1-x}Ga_xAs_yP_{1-y}$/InP double-heterostructure lasers emitting in the 1.3–1.7 $\mu$m wavelength region become a promising candidate for the light source of an optical fiber communication system because of recent development of low-loss, low-dispersion optical fibers in this spectral region. The $In_{1-x}Ga_xAs_yP_{1-y}$/InP system is also necessary for the efficient operation of a number of optoelectronic and transport devices, i.e., photodetectors, light emitting diodes, high-speed heterojunction transistors, etc.[1,2]

The band-gap energy in the $In_{1-x}Ga_xAs_yP_{1-y}$ quaternary and its dependence on the alloy compositions are known to be very important device parameters, and they have received considerable attention in the past.[3–7] Transport- and optoelectronic-device parameters in this system have, however, been hampered by a lack of definite knowledge of many various material parameters such as effective mass, dielectric constant, and deformation potential. This necessitates the use of some sort of an interpolation scheme. Recently, Olsen *et al.*[8] have obtained several material parameters of $In_{1-x}Ga_xAs_yP_{1-y}$ (band gap, lattice parameter, and refractive index) from an interpolation scheme and found good agreement with the experimental data. Such an interpolation scheme is essentially based on known values of the physical parameters for the related binary and ternary alloys.[9] Although the interpolation scheme is still open to experimental verification, it provides more useful and reliable material parameters over the entire range of alloy composition. However, some kinds of material parameters, e.g., lattice thermal conductivity,[10] exhibit strong nonlinearity with respect to the alloy composition which arises from the effects of alloy disorder. In such a case, attention must be carefully paid to the interpolated values.

The purpose of this paper is twofold: (1) to obtain various material parameters of $In_{1-x}Ga_xAs_yP_{1-y}$ quaternaries by using the interpolation methods, and (2) to discuss the acceptability of such interpolated parameters from an aspect of the solid-state physics. In Sec. II, we review several models available for calculating material parameters, based on the interpolation between such experimental data as are available for relevant binary and ternary materials. In Sec. III, we present and discuss various material parameters of $In_{1-x}Ga_xAs_yP_{1-y}$. The parameters considered in the present study are as follows:

(1) Lattice constant and crystal density
(2) Thermal expansion parameter
(3) Electronic-band structure
(4) Pressure and temperature dependences of the lowest-gap energy
(5) Effective mass
(6) Static and high-frequency dielectric constants
(7) Fröhlich (electron-phonon) coupling parameter
(8) Elastic properties
(9) Piezoelectric effect
(10) Deformation potential
(11) Excitonic effect

The key properties of such material parameters for a variety of $In_{1-x}Ga_xAs_yP_{1-y}$ device applications are also discussed in the text and Appendices. Finally, in Sec. IV, the conclusions obtained in the present study are summarized.

## II. INTERPOLATION METHOD

An interpolation scheme is known to be a useful tool for estimating some physical parameters of alloy compounds. If one uses the scheme, the ternary material parameter ($T$) can be derived from binary parameters ($B$'s) by

$$T_{ABC}(x) = xB_{AB} + (1-x)B_{AC} \equiv a + bx \quad (1)$$

 0021-8979/82/128775-18$02.40  

for alloys of the form: $AB_xC_{1-x}$, where $a \equiv B_{AC}$ and $b \equiv (B_{AB} - B_{AC})$. Some experimental data, however, deviate from linearity relation of Eq. (1), and have an approximately quadratic dependence on the mole fraction of one compound $x$:

$$T_{ABC}(x) = a + bx + cx^2, \tag{2}$$

where $c$ is referred to as a nonlinear or bowing parameter. The parameters $a$ and $b$ are determined by the values observed in the pure binary compounds. The parameter $c$ can be estimated by taking into account the virtual-crystal and disorder-scattering effects, and then it can be given by a sum of the intrinsic bowing $c_i$ found in the virtual-crystal approximation and the extrinsic bowing $C_e$ due to the effect of aperiodicity.[11] The material parameters such as the lattice constant vary linearly with composition $x$, and therefore Eq. (1) gives a good estimate for the relevant alloy-compound parameters. The parameters such as the lattice thermal conductivity, on the other hand, exhibit a strong quadratic dependence on the molar composition $x$, reflecting large value of the bowing $c$ in Eq. (2).

Quaternary material, $A_{1-x}B_xC_yD_{1-y}$, is thought to be constructed of four binary compounds: AC, AD, BC, and BD. The quaternary material parameter ($Q$) can, thus, be derived from the four binary parameters by using the interpolation scheme

$$Q(x,y) = (1-x)yB_{AC} + (1-x)(1-y)B_{AD} + xyB_{BC} + x(1-y)B_{BD}. \tag{3}$$

If one of the four binary parameters is lacking, the quaternary parameters can be obtained by the following expression:

$$Q(x,y) = xB_{BC} + (y-x)B_{AC} + (1-y)B_{AD}. \tag{4}$$

If relationships for the ternary material parameters are available, the quaternary parameter can be expressed as[12]

$$Q(x,y) = \frac{x(1-x)[(1-y)T_{ABD} + yT_{ABC}] + y(1-y)(1-x)[(1-x)T_{ACD} + xT_{BCD}]}{x(1-x) + y(1-y)}, \tag{5}$$

where the ternary parameter may include a quadratic dependence represented by Eq. (2). It might seem that Eq. (5) gives the most reliable quaternary parameters. However, unfortunately, a complete set of the ternary data are scarcely available at present. In the following, we obtain various physical parameters of $In_{1-x}Ga_xAs_yP_{1-y}$ from the binary data of GaAs, GaP, InAs, and InP by using the interpolation scheme and discuss the acceptability of such parameters from an aspect of the solid-state physics.

## III. RESULTS AND DISCUSSION

### A. Lattice constant and crystal density

The lattice constant "$a$" is known to obey well Vegard's law, i.e., to vary linearly with composition.[3] Figure 1 shows the three dimensional representation of the lattice constant for $In_{1-x}Ga_xAs_yP_{1-y}$ over the entire range of compositions ($0 \leqslant x \leqslant 1.0, 0 \leqslant y \leqslant 1.0$). The corners of the figure correspond to the values of binaries, as listed in Table I. The $In_{1-x}Ga_xAs_yP_{1-y}$ compounds form crystals with the zincblende arrangement. The bold lines in the figure are the loci of the lattice constants for compositions lattice-matched to the zincblende-type compounds, InP, GaAs, and ZnSe. The lattice-matching relations between the compositions $x$ and $y$ can be expressed as

$$x \simeq 0.47y \quad (0 \leqslant y \leqslant 1.0), \tag{6a}$$

or more rigidly

$$x \simeq \frac{0.1894y}{0.4184 - 0.013y} \quad (0 \leqslant y \leqslant 1.0) \tag{6b}$$

on InP substrate,

$$x \simeq \frac{1.00 + y}{2.08} \quad (0 \leqslant y \leqslant 1.0) \tag{7}$$

on GaAs substrate, and

$$x \simeq \frac{1.06 + y}{2.06} \quad (0 \leqslant y \leqslant 1.0) \tag{8}$$

on ZnSe substrate. Equations (6)–(8), in principle, provide lattice matching between $In_{1-x}Ga_xAs_yP_{1-y}$ and such substrates within $|\Delta a/a| < 0.032\%$.

Figure 2 shows the crystal density "$g$" as a function of the $y$-composition parameter for $In_{1-x}Ga_xAs_yP_{1-y}$ lattice-matched to InP obtained from the Vegard's relation, i.e., from Eq. (3). In this case, the Vegard's law gives correct

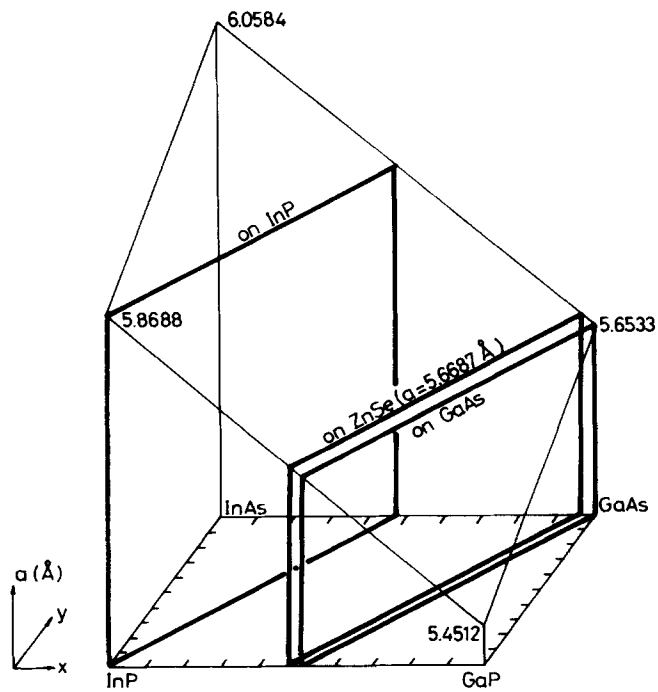


FIG. 1. Three-dimensional representation of the lattice constant for $In_{1-x}Ga_xAs_yP_{1-y}$ over the entire range of compositions.

TABLE I. Material parameters of GaAs, GaP, InAs, and InP.

| Parameter | GaAs | GaP | InAs | InP |
|---|---|---|---|---|
| $a$ (Å) | 5.6533[a] | 5.4512[a] | 6.0584[a] | 5.8688[a] |
| $g$† (g/cm$^3$) | 5.307 | 4.130 | 5.667 | 4.787 |
| $\alpha_{th}$ ($\times 10^{-6}$ °C$^{-1}$) | 6.63[a] | 5.91[a] | 5.16[a] | 4.56[b] |
| $E_0$ (eV) | 1.42[c,d] | 2.74[c,d] | 0.36[e] | 1.35[d] |
| $E_0+\Delta_0$ (eV) | 1.76[c,d] | 2.84[c,d] | 0.79[f] | 1.45[d] |
| $E_1$ (eV) | 2.925[d] | 3.75[d] | 2.50[d] | 3.155[d] |
| $E_1+\Delta_1$ (eV) | 3.155[d] | ... | 2.78[d] | 3.305[d] |
| $E_0'$ (eV) | 4.44[d] | 4.78[d] | 4.44[d] | 4.72[d] |
| $E_2$ (eV) | 4.99[d] | 5.27[d] | 4.70[d] | 5.04[d] |
| $E_2+\delta$ (eV) | 5.33[d] | 5.74[d] | 5.18[d] | 5.60[d] |
| $dE_0/dP$ ($\times 10^{-6}$ eV/bar) | 11.5[g] | 11.0[g] | 10.0[g] | 8.5[g] |
| $dE_0/dT$ ($\times 10^{-4}$ eV/deg) | $-3.95$[h] | $-4.6$[i] | $-3.5$[j] | $-2.9$[k] |
| $m^*$ | 0.067[l] | 0.17[l] | 0.023[l] | 0.08[l] |
| $m_{lh}^*$ | 0.074[l] | 0.14[l] | 0.027[l] | 0.089[l] |
| $m_{hh}^*$ | 0.62[l] | 0.79[l] | 0.60[l] | 0.85[l] |
| $m_{so}^*$ | 0.15[l] | 0.24[l] | 0.089[l] | 0.17[l] |
| $\epsilon_s$† | 13.1 | 11.1 | 14.6 | 12.4 |
| $\epsilon_\infty$† | 11.1 | 8.46 | 12.25 | 9.55 |
| $f_i$ | 0.310[m] | 0.327[m] | 0.357[m] | 0.421[m] |
| $\alpha_F$ | 0.07[n] | 0.20[n] | 0.05[n] | 0.08[n] |
| $C_{11}$ ($\times 10^{11}$ dyn/cm$^2$) | 11.88[o] | 14.120[p] | 8.329[q] | 10.22[r] |
| $C_{12}$ ($\times 10^{11}$ dyn/cm$^2$) | 5.38[o] | 6.253[p] | 4.526[q] | 5.76[r] |
| $C_{44}$ ($\times 10^{11}$ dn/cm$^2$) | 5.94[o] | 7.047[p] | 3.959[q] | 4.60[r] |
| $Y$† ($\times 10^{11}$ dyn/cm$^2$) | 8.53 | 10.28 | 5.14 | 6.07 |
| $P$† | 0.312 | 0.307 | 0.352 | 0.360 |
| $B$† ($\times 10^{11}$ dyn/cm$^2$) | 7.55 | 8.88 | 5.79 | 7.25 |
| $A$† | 0.547 | 0.558 | 0.480 | 0.485 |
| $e_{14}$ (C/m$^2$) | $-0.16$[s] | $-0.10$[t] | $-0.045$[s] | $-0.035$[u] |
| $K_{[110]}$ | 0.0617 | 0.0384 | 0.0201 | 0.0158 |
| $a$ (eV) | 2.7[v] | 3.0[v] | 2.5[v] | 2.9[v] |
| $b$ (eV) | $-1.7$[w] | $-1.5$[x] | $-1.8$[y] | $-2.0$[z] |
| $d$ (eV) | $-4.55$[w] | $-4.6$[x] | $-3.6$[y] | $-5.0$[z] |
| $\Xi_{\rm eff}$† (eV) | 6.74 | 6.10 | 6.76 | 7.95 |
| $G$† (meV) | 4.4 | 10.0 | 1.2 | 5.5 |
| $a_B$† (Å) | 136 | 48 | 406 | 106 |


[a] R. K. Willardson and A. C. Beer, *Semiconductors and Semimetals* (Academic, New York, 1966); H. Kressel and J. K. Butler, *Semiconductor Lasers and Heterojunction LED's* (Academic, New York, 1977).
[b] R. Bisaro, P. Merenda, and T. P. Pearsall, Appl. Phys. Lett. **34**, 100 (1979).
[c] A. G. Thompson, M. Cardona, and K. L. Shaklee, Phys. Rev. **146**, 601 (1966).
[d] M. Cardona, K. L. Shaklee, and F. H. Pollak, Phys. Rev. **154**, 696 (1967).
[e] R. E. Nahory, M. A. Pollack, W. D. Johnston, Jr., and R. L. Barns, Appl. Phys. Lett. **33**, 659 (1978).
[f] C. R. Pidgeon, S. H. Groves, and J. Feinleib, Solid State Commun. **5**, 677 (1967).
[g] R. Zallen and W. Paul, Phys. Rev. **155**, 703 (1967).
[h] M. Zvara, Phys. Status Solidi **27**, K157 (1968).
[i] R. Zallen and W. Paul, Phys. Rev. **134**, A1628 (1964).
[j] F. Matossi and F. Stern, Phys. Rev. **111**, 472 (1958).
[k] W. J. Turner, W. E. Reese, and G. D. Pettit, Phys. Rev. **136**, A1467 (1964).
[l] P. Lawaetz, Phys. Rev. B **4**, 3460 (1971).
[m] J. C. Phillips, *Bonds and Bands in Semiconductors* (Academic, New York, 1973).
[n] J. T. Devreese, *Polarons in Ionic Crystals and Polar Semiconductors* (North-Holland, Amsterdam, 1977).
[o] T. B. Bateman, H. J. McSkimin, and J. M. Whelan, J. Appl. Phys. **30**, 544 (1959).
[p] R. Weil and W. Groves, J. Appl. Phys. **39**, 4049 (1968).
[q] D. Gerlich, J. Appl. Phys. **34**, 2915 (1963).
[r] F. S. Hickernell and W. R. Gayton, J. Appl. Phys. **37**, 462 (1966).
[s] G. Arlt and P. Quadflieg, Phys. Status Solidi **25**, 323 (1968).
[t] D. F. Nelson and E. H. Turner, J. Appl. Phys. **39**, 3337 (1968).
[u] D. L. Rode, Phys. Rev. B **2**, 1012 (1970).
[v] J. D. Wiley, Solid State Commun. **8**, 1865 (1970).
[w] M. Chandrasekhar and F. H. Pollak, Phys. Rev. B **15**, 2127 (1977).
[x] H. Mathieu, P. Merle, E. L. Ameziane, B. Archilla, J. Camassel, and G. Poiblaud, Phys. Rev. B **19**, 2209 (1979).
[y] P. Y. Yu, M. Cardona, and F. H. Pollak, Phys. Rev. B **3**, 340 (1971).
[z] J. Camassel, P. Merle, L. Bayo, and H. Mathieu, Phys. Rev. B **22**, 2020 (1980).

† The data was gathered from many sources, or computed from the expressions given in the text.

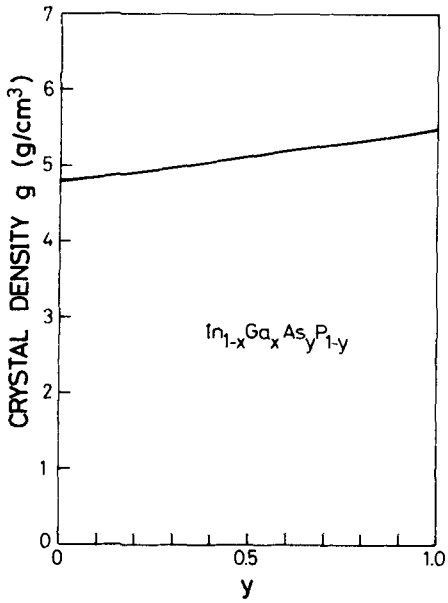


FIG. 2. Crystal density as a function of the $y$-composition parameter for $In_{1-x}Ga_xAs_yP_{1-y}$ lattice-matched to InP.

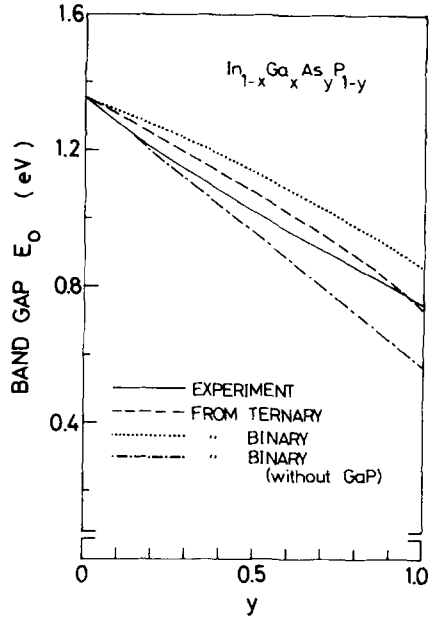


FIG. 4. The lowest-direct gap $E_0$ as a function of the $y$-composition parameter for $In_{1-x}Ga_xAs_yP_{1-y}$ lattice-matched to InP. Theoretical predictions were obtained from Eq. (3) [dotted line], Eq. (4) [dash-dotted line], and Eq. (5) [dashed line]. The solid line is the experimental data of Nahory *et al.* (Ref. 3).

physical values because their lattice constants remain exactly fixed to that of InP. The density varies almost linearly with $y$ from $g = 4.787$ g/cm$^3$ for InP ($y = 0$) to 5.499 g/cm$^3$ for $In_{0.53}Ga_{0.47}As$ ($y = 1.0$).

### B. Thermal expansion parameter

The $In_{1-x}Ga_xAs_yP_{1-y}$ quaternaries are thought to be promising materials for high-speed transistors and optoelectronic devices. The efficiency and performance of such devices depend on the defect level present in the material and how likely those defects are to be mobile under device operating conditions. A difference in the thermal expansion coefficient usually exists between the two different materials (heterojunction), and thus the lattice can be strained and dislocations may be produced. The difference in thermal expansion can also produce a driving force for the defects move in the heterojunctions. In Fig. 3, we show the thermal expansion coefficients ($\alpha_{th}$'s) as a function of the $y$-composition parameter for $In_{1-x}Ga_xAs_yP_{1-y}$ lattice-matched to InP, GaAs, and ZnSe. Recently, Bisaro *et al.*[13] have determined

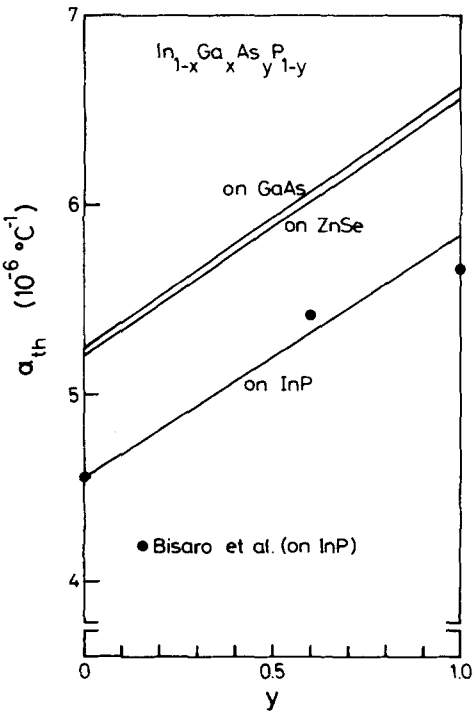


FIG. 3. Thermal expansion coefficients as a function of the $y$-composition parameter for $In_{1-x}Ga_xAs_yP_{1-y}$ lattice-matched to InP, GaAs, and ZnSe.

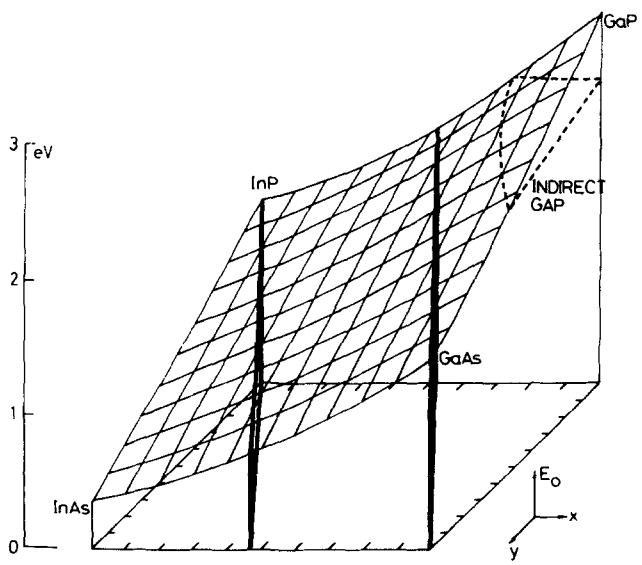


FIG. 5. Three-dimensional representation of the $In_{1-x}Ga_xAs_yP_{1-y}$ $E_0$-gap surface with $x$- and $y$-composition increments of 0.1.

the thermal expansion coefficients of $In_{1-x}Ga_xAs_yP_{1-y}$ ($y = 0$. 0.6, and 1.0) lattice-matched to InP. Their data are also shown in the figure by the solid circles. As clearly seen in Fig. 3, the values estimated from the interpolation scheme are in very good agreement with those obtained by Bisaro *et al.* The corresponding substrates data of $\alpha_{th}$ are as follows: $4.56\times10^{-6}\,°C^{-1}$ for InP [Ref. 13], $6.63\times10^{-6}\,°C^{-1}$ for GaAs [Ref. 14], and $7.0\times10^{-6}\,°C^{-1}$ for ZnSe [Ref. 15]. Thus, the present results suggest that for the $In_{1-x}Ga_xAs_yP_{1-y}$/GaAs (or ZnSe) systems the larger $y$-composition materials may, in principle, provide a better heterojunction quality, in contrast to the case for the $In_{1-x}Ga_xAs_yP_{1-y}$/InP systems (i.e., the smaller $y$-composition materials for the $In_{1-x}Ga_xAs_yP_{1-y}$/InP systems may provide a better heterojunction quality).

### C. Electronic-band structure

The electronic-band structure of $In_{1-x}Ga_xAs_yP_{1-y}$ quaternaries has been studied in detail by a number of groups.[3–7] A great deal of attention has been paid to the lowest-direct gap energy $E_0$ by reason of optoelectronic device applications. In contrast to the case of the lattice constant, in the III-V ternary systems the band-gap energy as a function of composition is known to be nonlinear and can be described by a quadratic in the composition parameter.[11] This fact suggests that the quaternary system has a complex relation between the band-gap energy and composition parameters. Figure 4 shows the lowest-direct gap $E_0$ as a function of the $y$-composition parameter for $In_{1-x}Ga_xAs_yP_{1-y}$ lattice-matched to InP. The theoretical predictions were ob-

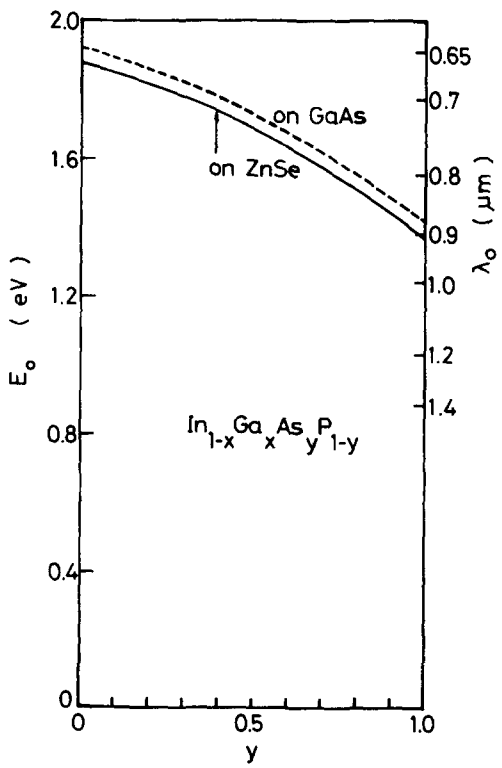


FIG. 6. $E_0$-gap energies as a function of the $y$-composition parameter for $In_{1-x}Ga_xAs_yP_{1-y}$ lattice-matched to GaAs and ZnSe.

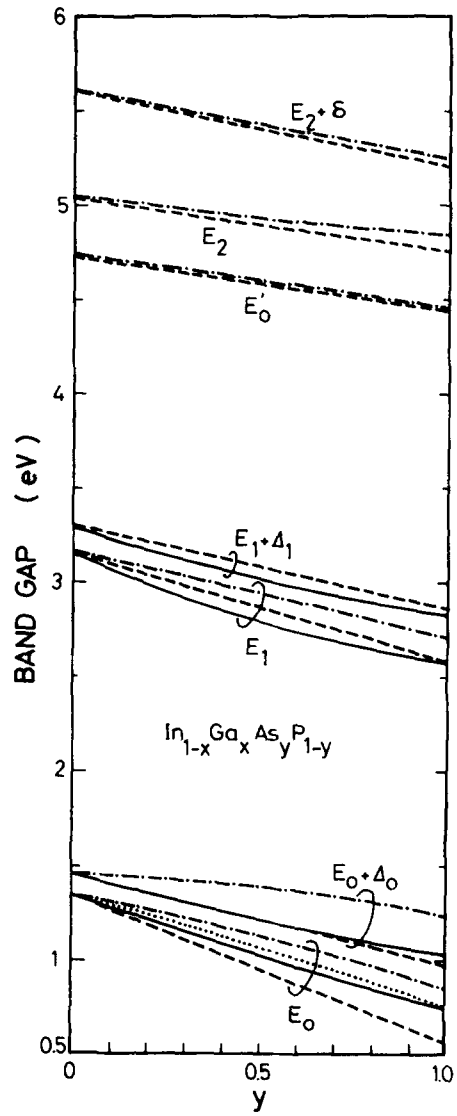


FIG. 7. A series of the critical points energies as a function of the $y$-composition parameter for $In_{1-x}Ga_xAs_yP_{1-y}$ lattice-matched to InP [see text].

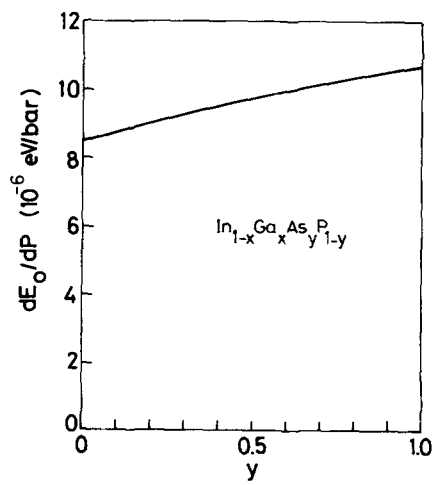


FIG. 8. Hydrostatic-pressure dependence of the $E_0$-gap energy as a function of the $y$-composition parameter for $In_{1-x}Ga_xAs_yP_{1-y}$ lattice-matched to InP.

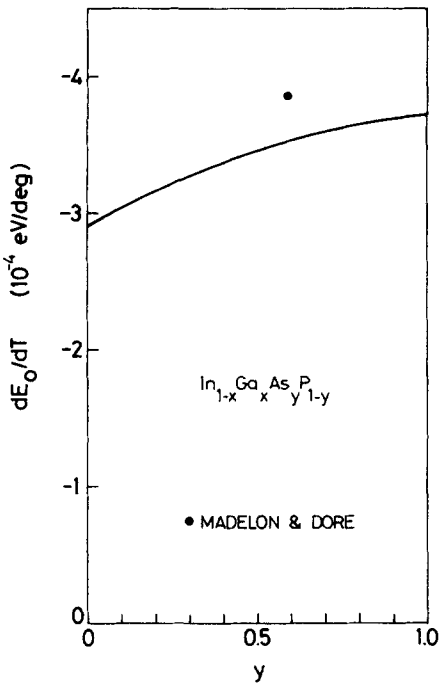


FIG. 9. Temperature dependence of the $E_0$-gap energy as a function of the $y$-composition parameter for $In_{1-x}Ga_xAs_yP_{1-y}$ lattice-matched to InP. The solid circle is the experimental data obtained from derivative transmission measurements by Madelon and Dore (Ref. 7).

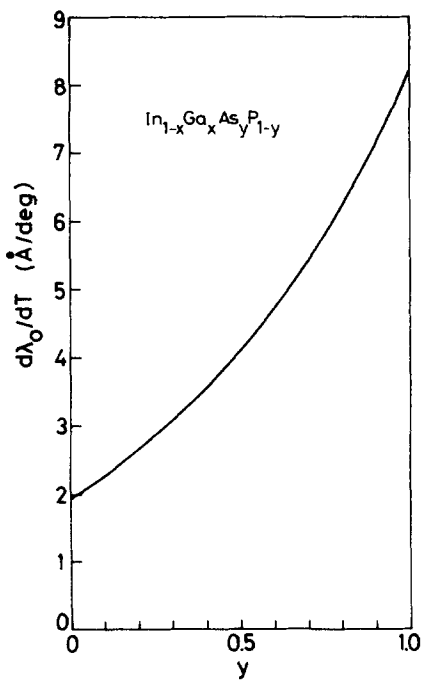


FIG. 10. Temperature dependence of the lasing wavelength as a function of the $y$-composition parameter for $In_{1-x}Ga_xAs_yP_{1-y}$ lattice-matched to InP.

tained from Eq. (3) [dotted line], Eq. (4) [dash-dotted line], and Eq. (5) [dashed line]. The compositional-dependence data of $E_0$ in the ternary systems used are as follows[16]:

$$E_0(In_{1-x}Ga_xP) = 1.35 + 0.643x + 0.786x^2, \quad (9a)$$

$$E_0(In_{1-x}Ga_xAs) = 0.36 + 0.505x + 0.555x^2, \quad (9b)$$

$$E_0(InAs_yP_{1-y}) = 1.35 - 1.083y + 0.091y^2, \quad (9c)$$

$$E_0(GaAs_yP_{1-y}) = 2.74 - 1.473y + 0.146y^2. \quad (9d)$$

The binary data used are listed in Table I. The solid line is the experimental data of Nahory *et al.*[3] who give the compositional dependence of $E_0$ as

$$E_0(y) = 1.35 - 0.72y + 0.12y^2. \quad (10)$$

As clearly seen in Fig. 4, the $E_0$-gap energies estimated from Eq. (5) are in better agreement with the experimental data than those from Eqs. (3) and (4). However, an obvious discrepancy still exists between the interpolated values of Eq. (5) and experimental data which is though to be due to the effects of quaternary-alloy disorder. If one assumes that the degree of alloy disorder is proportional to $x(1-x)$ (ternary) or $x(1-x)+y(1-y)$ (quaternary), it becomes maximum at $x=0.5$ for the ternary systems and at $y\simeq 0.6$ for $In_{1-x}Ga_xAs_yP_{1-y}$ lattice-matched to InP. This simple consideration well interprets the disorder effects on the lattice thermal conductivity in the ternaries[10] and quaternaries.[17]

Figure 5 shows the three-dimensional representation of the $In_{1-x}Ga_xAs_yP_{1-y}$ $E_0$-*gap* surface with $x$- and $y$-composition increments of 0.1. The curves are obtained from the interpolation scheme of Eq. (5). The $E_0$-gap energies as a function of the $y$-composition parameter for $In_{1-x}Ga_xAs_yP_{1-y}$ lattice-matched to GaAs and ZnSe are also shown in Fig. 6. These systems, especially $In_{1-x}Ga_xAs_yP_{1-y}$/ZnSe systems, may enable to fabricate visible-spectrum semiconductor lasers in the wavelength range 0.65–0.9 $\mu$m. The $In_{1-x}Ga_xAs_yP_{1-y}$/ZnSe systems provide large enough band-gap differences and refractive-index steps between $In_{1-x}Ga_xAs_yP_{1-y}$ and ZnSe for the injected-carrier and light confinements in heterostructures (see Appendix A).

A series of the critical-points energies can also be obtained by using the interpolation schemes. Figure 7 shows the calculated critical-points energies of $E_0$, $E_0+\Delta_0$, $E_1$, $E_1+\Delta_1$, $E_0'$, $E_2$, and $E_2+\delta$ versus $y$ for $In_{1-x}Ga_xAs_yP_{1-y}$ lattice-matched to InP, along with the experimental data (solid lines).[5] The dash-dotted lines are from Eq. (3), the dashed lines from Eq. (4), and the dotted line is from Eq. (5).

### D. Pressure and temperature dependences of the $E_0$-gap energy

The hydrostatic-pressure and temperature dependences of the $E_0$-gap energies as a function of the $y$-composition parameter for $In_{1-x}Ga_xAs_yP_{1-y}$ lattice-matched to InP are shown in Figs. 8 and 9, respectively. The solid circle in Fig. 9 is the experimental data obtained from derivative transmission measurements by Madelon and Dore.[7] The pressure coefficients ($dE_0/dP$), which characterized the principal [000] conduction-band minima, were in the range of $8.50$–$10.70\times10^{-6}$ eV/bar between $y=0$ (InP) and 1.0 ($In_{0.53}Ga_{0.47}As$). The temperature coefficient ($dE_0/dT$) is known to be linear for temperatures higher than 150 K, as in most of the semiconductors. The derivative-transmission data ($dE_0/dT\simeq -3.87\times10^{-4}$ eV/deg at $y=0.59$)[7] is thought to be in good agreement with the interpolated value

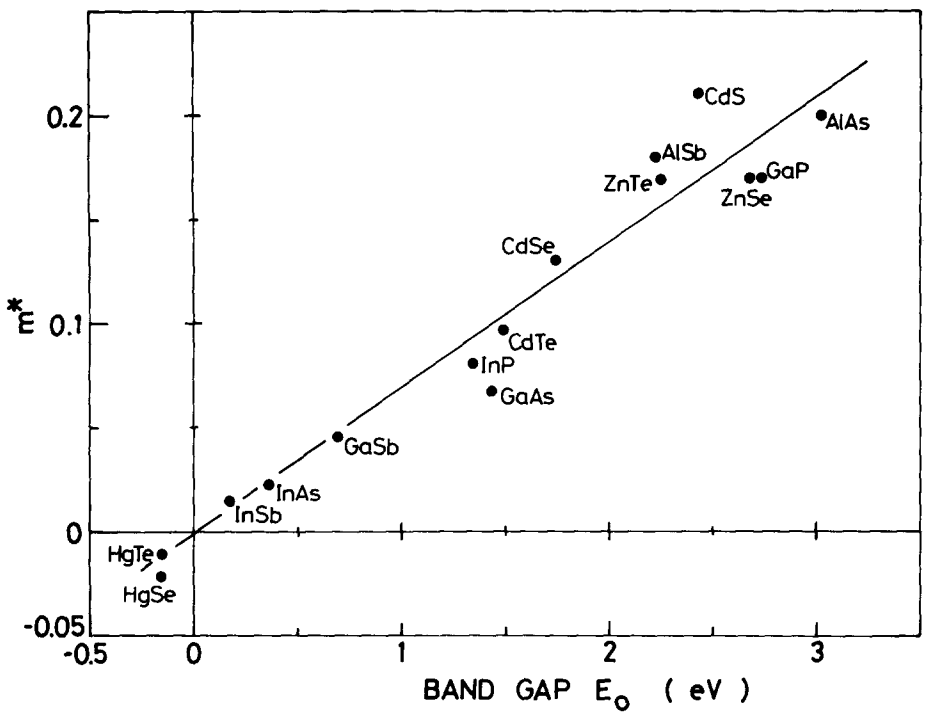


FIG. 11. Effective mass, $m^*$, as a function of the lowest-direct gap $E_0$ for a number of the III-V and II-VI compounds.

($\simeq -3.52\times10^{-4}$ eV/deg). Assuming that $In_{1-x}Ga_xAs_yP_{1-y}$/InP laser wavelengths $\lambda_0$ correspond to the $In_{1-x}Ga_xAs_yP_{1-y}$ active-layer band energies $E_0(y)$, one can also calculate the temperature dependence of the lasing wavelength. The results are shown in Fig. 10. Arai *et al.*[18] have recently measured the temperature dependence of lasing wavelengths for InGaAsP/InP double-heterostructure lasers in the range of 1.24–1.67 $\mu$m. They reported $d\lambda_0/dT\simeq4$ Å at $\lambda_0 = 1.3$ $\mu$m ($y\simeq0.6$) and $\simeq5$ Å at $\lambda_0\simeq1.55$ $\mu$m ($y\simeq0.9$) [Fig. 13 in Ref. 18], in reasonable agreement with the present calculation [Note that the ratio $d\lambda_0/dT$ depends not only on the $y$-composition parameters, but also on the injected-carrier levels and/or laser structures]. The predicted values of $d\lambda_0/dT$ have a linear relation with respect to $\lambda_0$, similar to the measured values.[18]

### E. Effective mass

To analyze a number of important semiconductor properties, it is required quite detailed knowledge of band parameters at the principal band extrema. The effective mass, which is strongly connected with the carrier mobility,[19–22] is known to be one of the most important device parameters. It has, thus, recently received considerable attention in the quaternary $In_{1-x}Ga_xAs_yP_{1-y}$ system for the prediction of the transport properties in this material.[23] Particular attention has been paid to the study of the dependence of effective mass upon alloy composition in this system.[24–29] The measurements used a variety of techniques, such as Shubnikov-de Haas effect, magnetophonon resonance, cyclotron resonance, and interband magnetoabsorption.

The $k\cdot p$ method is a powerful procedure for evaluating the band parameters in the vicinity of some important point in $\vec{k}$ space. The three-level $k\cdot p$ analysis at $\vec{k}=0$ in the zinc-blende-type semiconductors gives[30]

$$\frac{1}{m^*} = 1 + \frac{P^2}{3}\left(\frac{2}{E_0} + \frac{1}{E_0+\Delta_0}\right), \tag{11}$$

where $m^*$ is the electron effective mass and $P^2$ is the interband squared $P$-matrix element. Assuming that $E_0 \gg \Delta_0$ and $1/m^* \gg 1$, Eq. (11) can be written as

$$\frac{1}{m^*} \simeq \frac{P^2}{E_0}. \tag{12}$$

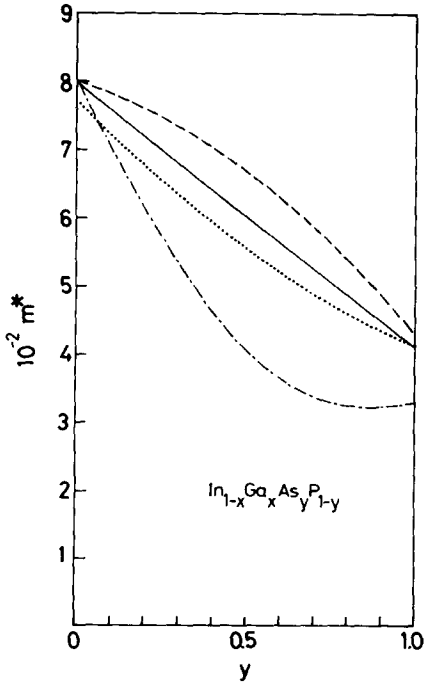


FIG. 12. Effective mass, $m^*$, as a function of the $y$-composition parameter for $In_{1-x}Ga_xAs_yP_{1-y}$ lattice-matched to InP [see text].

If one also assumes that $P^2$ is independent of material, $m^*$ is directly related to the lowest-direct gap $E_0$. Figure 11 shows the values of $m^*$ as a function of $E_0$ for a number of the III-V and II-VI binary compounds. The relation between $m^*$ and $E_0$ in Fig. 11, in fact, shows a good agreement with that predicted from Eq. (12).

We now discuss the electron effective mass of the quaternary $In_{1-x}Ga_xAs_yP_{1-y}$ lattice-matched to InP. The mass $m^*$ is shown as a function of the $y$-composition parameter in Fig. 12, as deduced from the measurements. There was some discrepancy between the experimental results. Restorff *et al.*[24] have obtained from the four ternary interpolations in the relation (dash-dotted line):

$$m^* = 0.08 - 0.116x + 0.026y - 0.059xy + (0.064 - 0.02x)y^2 + (0.06 + 0.032y)x^2. \quad (13)$$

Perea *et al.*[29] have also obtained a quadratic dependence (dotted line):

$$m^* = 0.077 - 0.050y + 0.014y^2. \quad (14)$$

The recent publication[27] has pointed out that the generally acceptable $m^*$ value is a linear relationship (solid line):

$$m^* = 0.080 - 0.039y. \quad (15)$$

Nicholas *et al.*[27,31] have also obtained the values of $m^*$ from the $k\cdot p$ theory. An obvious discrepancy, however, exists between the $k\cdot p$ calculation and experiment which is thought to be due to the effects of alloy disorder. Theoretical $m^*$ values can also be obtained by using the interpolation scheme [Eq. (3)] from the masses of the related binaries, as shown in Fig. 12 by the dashed line. It is clear that there is a deviation from the experimental data which may also be due to the effects of alloy disorder. Nicholas *et al.*[32] have measured cyclotron resonance and infrared absorption in the complete range of alloys $InAs_yP_{1-y}$ in the region of the direct gap, and have obtained that the effective masses are almost linear function of the alloy composition. This is in contrast to the prediction of the $k\cdot p$ theory (i.e., it predicts a strong bowing in $m^*$). They suggested that the discrepancy is thought to arise from a bowing in $P^2$.

The electron effective mass is rather accurately known from numerous experiments, but the valence-band masses must essentially be calculated from band theory. This approach was made by Lawaetz[33] for diamond- and zinc-blende-type semiconductors. Figure 13 shows the valence-band masses (light-hole mass $m_{lh}^*$, heavy-hole mass $m_{hh}^*$, and split-off band mass $m_{so}^*$) for $In_{1-x}Ga_xAs_yP_{1-y}$ lattice-matched to InP. These curves were obtained by using the interpolation scheme from the Lawaetz's binary values. Also shown in Fig. 13 are determinations of the light-hole mass deduced from spin-polarized photoluminescence by Hermann and Pearsall.[34]

Suematsu and co-workers[35] have suggested the posibility of new optical absorption in the $In_{1-x}Ga_xAs_yP_{1-y}$/InP laser due to electronic transitions between the split-off $\Gamma_7$- and degenerate $\Gamma_8$-valence bands. This absorption should determine the threshold condition of lasers through optical-loss mechanisms. With the aid of van Hove's critical-point analysis[36] and valence-band masses obtained here, we can obtain a detailed information on the optical absorption mechanisms due to electronic transitions between the $\Gamma$-point valence bands. Details are presented in Appendix B.

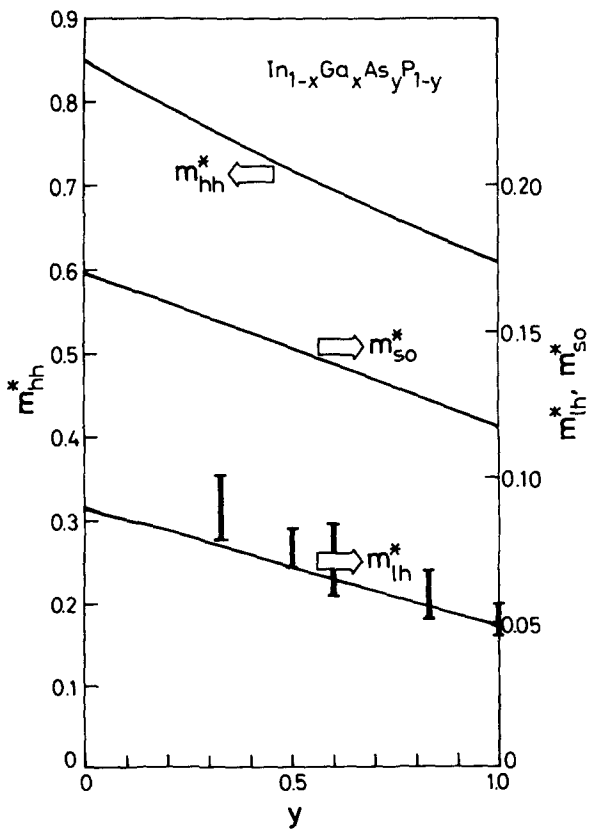


FIG. 13. Valence-band light-hole mass $m_{lh}^*$, heavy-hole mass $m_{hh}^*$, and split-off mass $m_{so}^*$, for $In_{1-x}Ga_xAs_yP_{1-y}$ lattice-matched to InP.

## F. Static and high-frequency dielectric constants

The concept of the dielectric behavior of solids is an old one which arose in strong connection with the electron-device properties.[37] We shall first sketch the dielectric constant

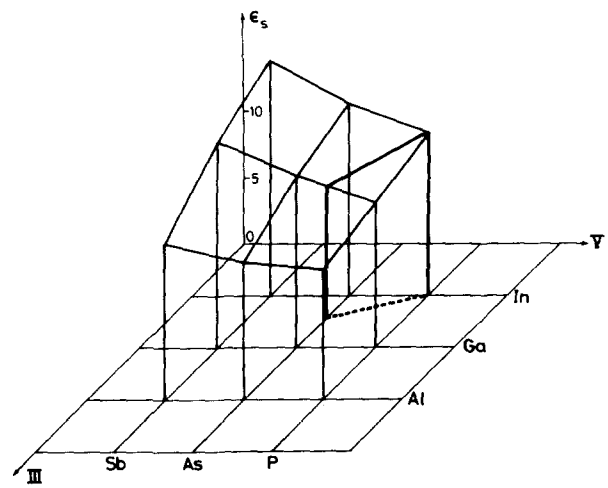


FIG. 14. Three-dimensional diagram indicating variation of the static dielectric constants $\epsilon_s$ with composition of III-V compounds.

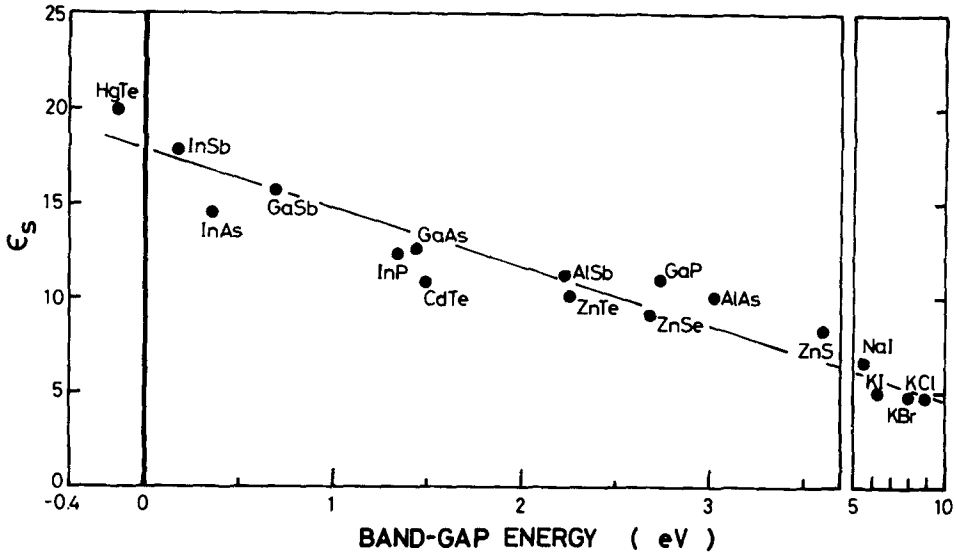


FIG. 15. Static dielectric constant $\epsilon_s$ as a function of the lowest-direct gap $E_0$ for some of the III-V, II-VI compounds, and alkali halides.

of specific family of binary compounds, namely the III-V and II-VI compounds, from a simplified point of view.

Figure 14 shows the three-dimensional diagram indicating variation of the static dielectric constants, $\epsilon_s$, with composition of III-V compounds. The dielectric constants $\epsilon_s$ of III-V compounds always increase with the atomic number of the compound, as can be easily understood from Fig. 14. The static dielectric constant $\epsilon_s$ as a function of the lowest-direct gap $E_0$ for some of the III-V, II-VI compounds, and alkali halides are also shown in Fig. 15. One can find from the figure that $\epsilon_s$ decreases with increasing $E_0$-gap energy. Phillips's ionicity theory[38] has been applied successfully to calculate various properties, such as ionization potential and cohesive energy, of a large number of covalent and ionic compounds. The value of $\epsilon_s$ can now be written as[36]

$$\epsilon_s = \epsilon_\infty + \frac{4\pi N e_T^2}{\omega_{TO}^2 M}, \tag{16}$$

where $\epsilon_\infty$ is the high-frequency dielectric constant (which will be mentioned next), $M$ the mass of atom, $N$ the number of atoms, $e_T$ the effective electrical charge, and $\omega_{TO}$ is the transverse optical phonon frequency. It is thought possible that $\epsilon_s$ has any relationship with the crystal ionicity, or the ionic character, which characterize fundamental properties and structures of solids. The values of $\epsilon_s$ for some of IV, III-

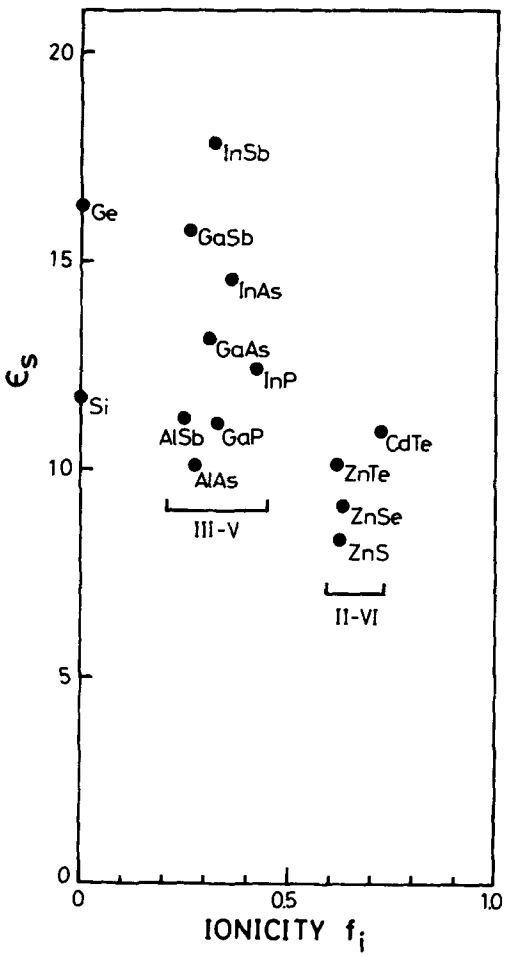


FIG. 16. Values of $\epsilon_s$ for some of the VI, III-V, and II-VI semiconductors with respect to the corresponding Phillips's ionicities.

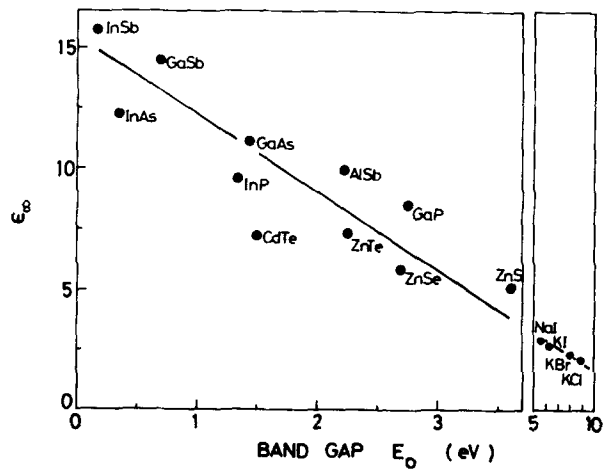


FIG. 17. High-frequency dielectric constant $\epsilon_\infty$ as a function of the lowest-direct gap $E_0$ for some of the III-V, II-VI compounds, and alkali halides.

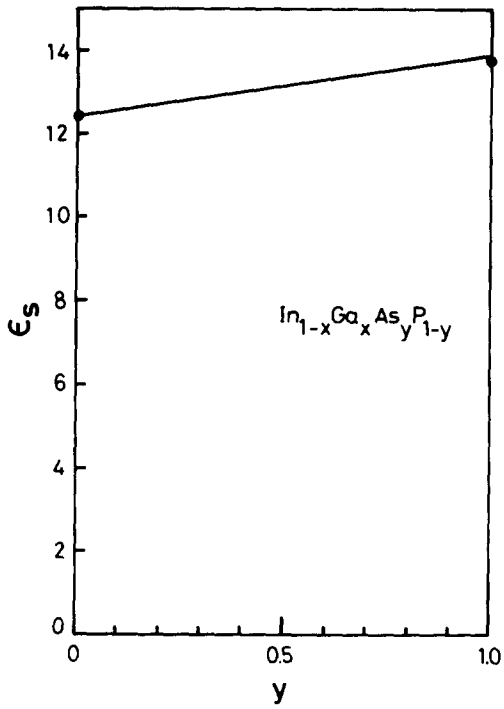


FIG. 18. Static dielectric constant $\epsilon_s$ as a function of the $y$-composition parameter for $In_{1-x}Ga_xAs_yP_{1-y}$ lattice-matched to InP.

V, and II-VI semiconductors are shown in Fig. 16 with respect to the corresponding Phillips's ionicities.[38] Though the values of $\epsilon_s$ vary within a family, one can recognize that there is a monotonic decrease in $\epsilon_s$ from the covalent group IV materials (Si and Ge), to the III-V, to the II-VI compounds, and to the much more ionic alkali halides ($\epsilon_s \simeq 5$).

The high-frequency dielectric constant $\epsilon_\infty$ has essentially the same behaviors as $\epsilon_s$. Figure 17 shows, as a verification, the values of $\epsilon_\infty$ as a function of the lowest-direct gap

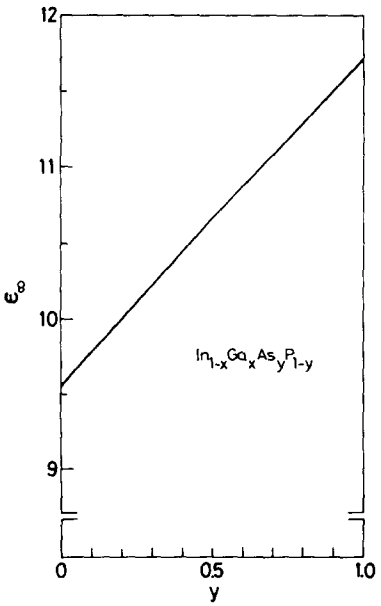


FIG. 19. High-frequency dielectric constant $\epsilon_\infty$ as a function of the $y$-composition parameter for $In_{1-x}Ga_xAs_yP_{1-y}$ lattice-matched to InP.

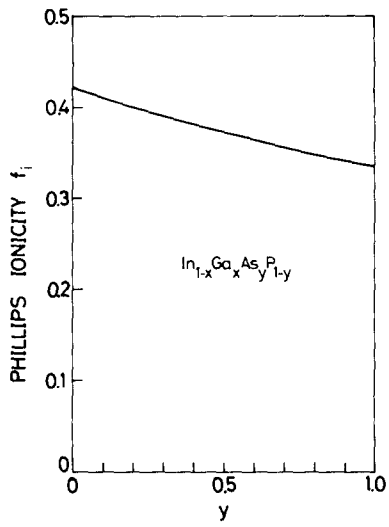


FIG. 20. Phillips's ionicity $f_i$ as a function of the $y$-composition parameter for $In_{1-x}Ga_xAs_yP_{1-y}$ lattice-matched to InP.

$E_0$ for some of the III-V, II-VI compounds, and alkali halides. The value of $\epsilon_\infty$ decreases with increasing $E_0$-gap energy, in fact, similar to the case of $\epsilon_s$.

By the aid of general trends obtained above and by the use of the interpolation scheme, we shall present the dielectric constants, $\epsilon_s$ and $\epsilon_\infty$, for $In_{1-x}Ga_xAs_yP_{1-y}$ lattice-matched to InP. The dielectric constants, $\epsilon_s$ and $\epsilon_\infty$, as a function of the $y$-composition parameter for $In_{1-x}Ga_xAs_yP_{1-y}$ are shown in Figs. 18 and 19, respectively. The interpolated value of $\epsilon_s$, as a function of $y$, is almost linear relationship given by

$$\epsilon_s(y) = 12.40 + 1.5y. \tag{17}$$

The solid circle in Fig. 18 is the value used frequently ($\epsilon_s = 13.77$ for $y = 1.0$).[21] The value of $\epsilon_\infty$ is also a linear relationship:

$$\epsilon_\infty(y) = 9.55 + 2.2y. \tag{18}$$

The $E_0$-gap energy, as a function of $y$, for $In_{1-x}Ga_xAs_yP_{1-y}$ lattice-matched to InP is nearly linear relationship, shown already in Fig. 4. The Phillips's ionicity $f_i$,[38] deduced from the interpolation scheme, is also a linear relationship, shown in Fig. 20. These $E_0$-gap and $f_i$ parameters decrease with increasing the $y$-composition parameter. The qualitative natures of the $\epsilon_s$ and $\epsilon_\infty$ constants in the $In_{1-x}Ga_xAs_yP_{1-y}$ system can, thus, be regarded to agree with the general trends derived before (Figs. 15–17).

### G. Fröhlich coupling parameter

It is known that the coupling between the electron and longitudinal-optical lattice vibration can not be neglected in the study of transport and optical properties in polar semiconductors.[39] The interaction between the electron and longitudinal optical phonons can be given by the well-known Fröhlich coupling constant:[40]

$$\alpha_F = \frac{1}{2} \frac{e^2/(\hbar/2m^*\omega_{LO})^{1/2}}{\hbar\omega_{LO}} \left[ \frac{1}{\epsilon_\infty} - \frac{1}{\epsilon_s} \right], \tag{19}$$

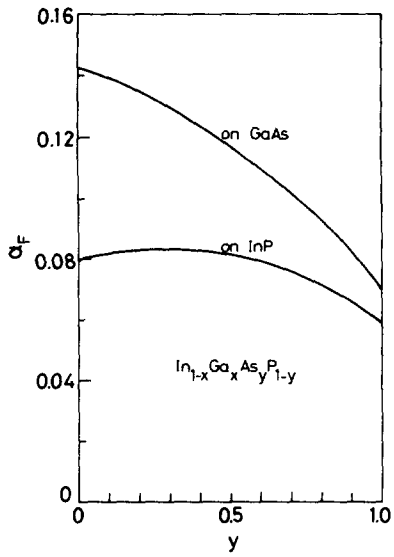


FIG. 21. Fröhlich coupling parameter $\alpha_F$ as a function of the $y$-composition parameter for $In_{1-x}Ga_xAs_yP_{1-y}$ lattice-matched to InP and GaAs.

where $\hbar\omega_{LO}$ is the longitudinal-optical phonon energy. One can see that this constant depends strongly on the ionic polarization of the crystal which is related to the dielectric constants $\epsilon_\infty$ and $\epsilon_s$. The interpolated $\alpha_F$'s, as a function of the $y$-composition proportion, for $In_{1-x}Ga_xAs_yP_{1-y}$ lattice-matched to InP and GaAs, are shown in Fig. 21. As seen in the figure, the $y$-composition dependence of $\alpha_F$ shows a relatively remarkable nonlinearity. There are no rigorous theoretical treatment related to the polaron interaction in alloys. To obtain accurate values of $\alpha_F$ in the alloy system, we must take into account the effects of multi LO phonons present. The case of ternary alloys where two LO phonon modes exist has been considered recently by Nicholas *et al.*[41] who defined a value of $\alpha_F$ for each LO phonon.

### H. Elastic properties

The quaternary $In_{1-x}Ga_xAs_yP_{1-y}$ and related binaries crystallize in the zincblende-type structure, and so the elastic stiffness tensor $[C]$ takes in the form[42]:

$$[C] = \begin{bmatrix} C_{11} & C_{12} & C_{12} & 0 & 0 & 0 \\ C_{12} & C_{11} & C_{12} & 0 & 0 & 0 \\ C_{12} & C_{12} & C_{11} & 0 & 0 & 0 \\ 0 & 0 & 0 & C_{44} & 0 & 0 \\ 0 & 0 & 0 & 0 & C_{44} & 0 \\ 0 & 0 & 0 & 0 & 0 & C_{44} \end{bmatrix}. \quad (20)$$

The elastic constants of the III-V binaries have been extensively measured, while to our knowledge only one is reported up to date for the ternary crystal.[43] The elastic constant can be contributed to the long-range Coulomb forces in solids. Thus, it seems that the elastic constant of ternaries is a linear with the composition proportion. In fact, the data for $C_{ij}$ of $In_{1-x}Ga_xP$[43] are successfully interpreted by the linear interpolation scheme, namely by Eq. (1). This supports that the interpolation given by Eq. (3) also provides reliable elastic parameters for the quaternary system.

The elastic stiffness components, $C_{11}$, $C_{12}$, and $C_{44}$, as a function of the $y$-composition proportion for $In_{1-x}Ga_xAs_yP_{1-y}$ lattice-matched to InP are shown in Fig. 22. The constants slowly vary with the $y$-composition proportion. The macroscopic theory of the elastic properties of solids is described in detail in tensor notation by Nye.[42] The elastic compliance tensor $[S]$, which has the same form as Eq. (20), is connected reciprocally with the tensor $[C]$ through Hook's relation. Explicit equations for the component $S_{ij}$ in terms of $C_{ij}$ can be given in the following equation:

$$S_{11} = \frac{C_{11} + C_{12}}{(C_{11} - C_{12})(C_{11} + 2C_{12})}, \quad (21a)$$

$$S_{12} = \frac{-C_{12}}{(C_{11} - C_{12})(C_{11} + 2C_{12})}, \quad (21b)$$

$$S_{44} = \frac{1}{C_{44}}. \quad (21c)$$

Young's modulus, $Y$, is not isotropic in the cubic zincblende-type crystals.[42] The variation, thus, depends on the direction of the crystal axes. The modulus $Y$ for the direction of the cube axes $\langle 100 \rangle$ is given by

$$Y = 1/S_{11}. \quad (22)$$

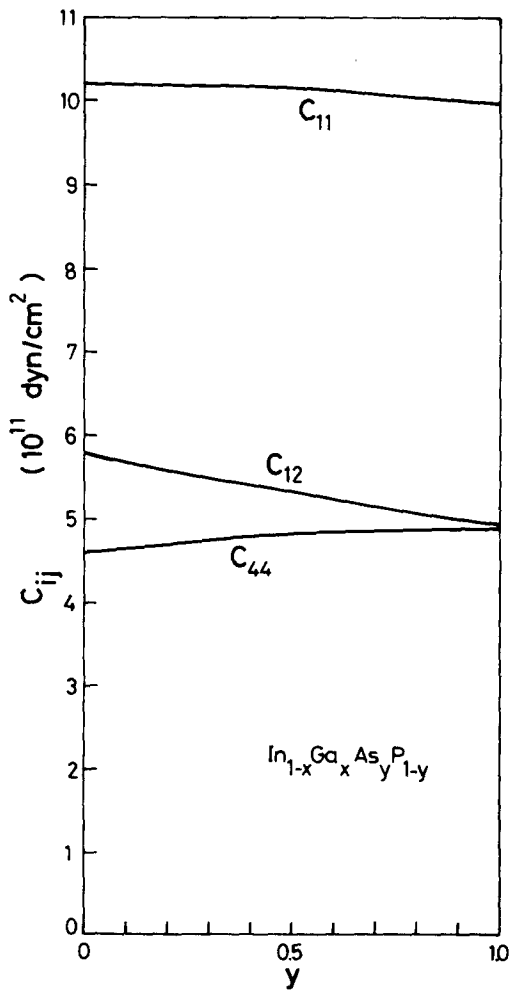


FIG. 22. Elastic stiffness constants, $C_{11}$, $C_{12}$, and $C_{44}$, as a function of the $y$-composition parameter for $In_{1-x}Ga_xAs_yP_{1-y}$ lattice-matched to InP.

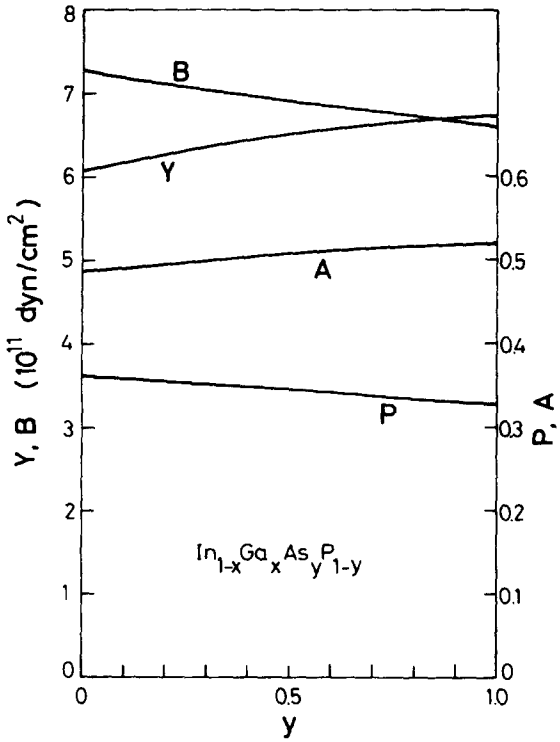


FIG. 23. Young's modulus $Y$, Poisson's ratio $P$, bulk modulus $B$, and anisotropy factor $A$, as a function of the $y$-composition parameter for $In_{1-x}Ga_xAs_yP_{1-y}$ lattice-matched to InP.

Poisson's ratio $P$, in this case, is written as

$$P = -S_{12}/S_{11}. \tag{23}$$

The bulk modulus, $B$, and anisotropy factor, $A$, for the zincblende-type crystals are, respectively, given by

$$B = (C_{11} + 2C_{12})/3, \tag{24}$$

and

$$A = (C_{11} - C_{12})/2C_{44}. \tag{25}$$

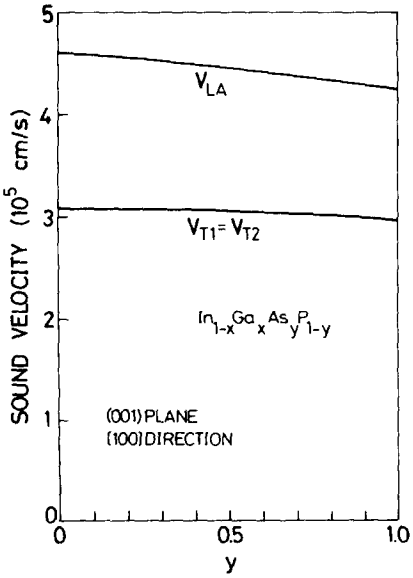


FIG. 24. Variation of the sound velocities propagating in the [100] direction in $In_{1-x}Ga_xAs_yP_{1-y}$ lattice-matched to InP.

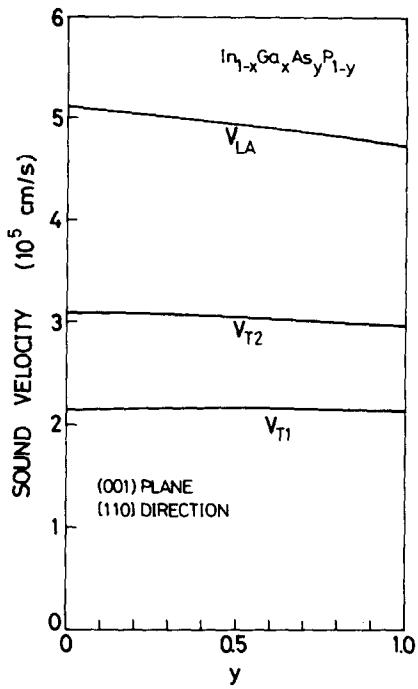


FIG. 25. Variation of the sound velocities propagating in the [110] direction in $In_{1-x}Ga_xAs_yP_{1-y}$ lattice-matched to InP.

In Fig. 23, we show the parameters, $Y$, $P$, $B$, and $A$, as a function of the $y$-composition parameter, for $In_{1-x}Ga_xAs_yP_{1-y}$ lattice-matched to InP. As can be seen, the parameters $P$ and $B$ decrease with increasing $y$, while the parameters $Y$ and $A$ increase with increasing $y$.

If the density ($g$) and stiffness constant ($C_{ij}$) of solids are known, one can calculate the sound velocity, $v$, from the general relation:

$$v = (C_{ij}/g)^{1/2}. \tag{26}$$

Figures 24 and 25 show the variation of the wave velocities in $In_{1-x}Ga_xAs_yP_{1-y}$ lattice-matched to InP propagating in the [100] and [110] directions, respectively. The data of $g$ and $C_{ij}$ were taken from Figs. 2 and 22, respectively. $v_{LA}$ corresponds to the longitudinal-wave mode velocity, $v_{T1}$ the slow transverse-wave mode velocity, and $v_{T2}$ corresponds to the fast transverse-wave mode velocity. One can find from the figures that the transverse-mode velocities vary slower than the longitudinal-wave one.

## I. Piezoelectric effect

An important aspect of the zincblende arrangement is the absence of a center of symmetry or inversion. The III-V compounds crystallizing in the zincblende-type structure are the simplest crystals lacking a center of symmetry and, hence, capable of exhibiting piezoelectric and related effects depending on polar symmetry. The piezoelectric tensor in the zincblende-type crystals ($\bar{4}3m$) has the following form[42]:

$$[e] = \begin{bmatrix} 0 & 0 & 0 & e_{14} & 0 & 0 \\ 0 & 0 & 0 & 0 & e_{14} & 0 \\ 0 & 0 & 0 & 0 & 0 & e_{14} \end{bmatrix}. \tag{27}$$

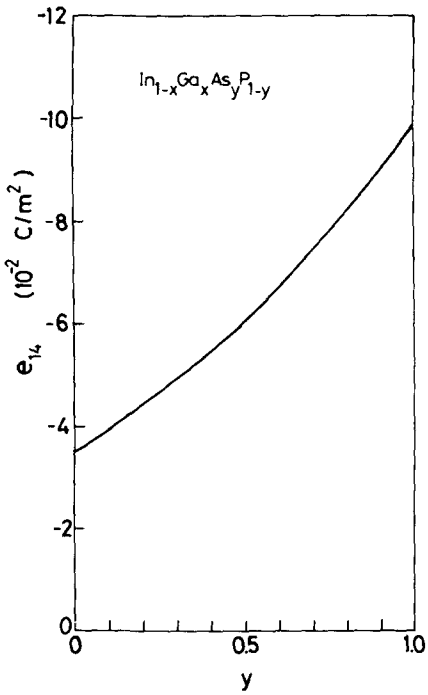


FIG. 26. Piezoelectric constant $e_{14}$ as a function of the $y$-composition parameter for $In_{1-x}Ga_xAs_yP_{1-y}$ lattice-matched to InP.

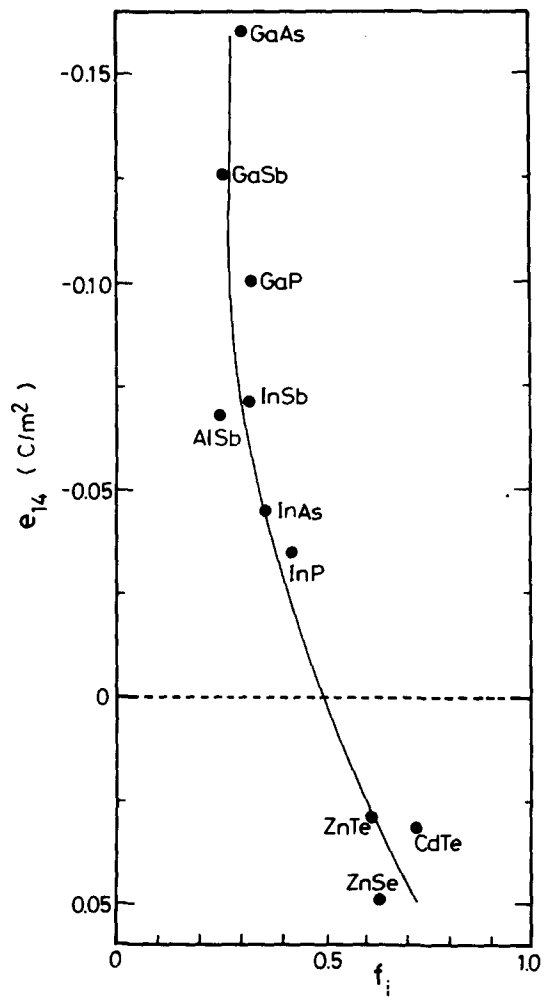


FIG. 27. Plots of $e_{14}$ vs Phillips's ionicity $f_i$ for some of the III-V and II-VI compounds.

The piezoelectric effect produces an important part in the study of transport properties in semiconductors.[39] The piezoelectric scattering of electrons in solids is usually not of major practical importance, except in high-quality crystals, because of impurity scattering. At low temperatures ($\lesssim 50$ K), however, lattice scattering of electrons is known to be dominated by the piezoelectric interaction, which causes elastic scattering due to the relatively low-energy acoustic phonons.[19,44]

The interpolated piezoelectric constant, $e_{14}$, versus $y$ for $In_{1-x}Ga_xAs_yP_{1-y}$ lattice-matched to InP is shown in Fig. 26. The data of the binaries used in the calculation are listed in Table I. It is noteworthy that the experimental data for $e_{14}$ of zincblende-type crystals reverse sign on going from the III-V to the II-VI binary compounds. Many theoretical attempts[45–47] have been made to understand this sign reversal. Based on a recent theory of Miura *et al.*,[47] we assumed the sign of $e_{14}$ for the III-V binaries to be negative and, as a result, for the III-V quaternaries to be the same as that for the binaries (i.e., negative). As can be seen, the value of $e_{14}$ for $In_{1-x}Ga_xAs_yP_{1-y}$ depends strongly on the $y$-composition proportion.

Arlt and Quadflieg[45] have measured piezoelectric constants for a variety of materials and have proposed the microscopic origins of piezoelectricity as being due to such as ionic polarization, strain-dependent ionicity, and electronic polarization. The plots of $e_{14}$ versus Phillips's ionicity $f_i$ for some of the III-V and II-VI compounds are shown in Fig. 27. One can easily understand that $e_{14}$ of materials passes through zero at $f_i \simeq 0.5$ while undergoing a reversal in sign. However, the reason why at $f_i \simeq 0.5$ $e_{14}$ becomes zero is not

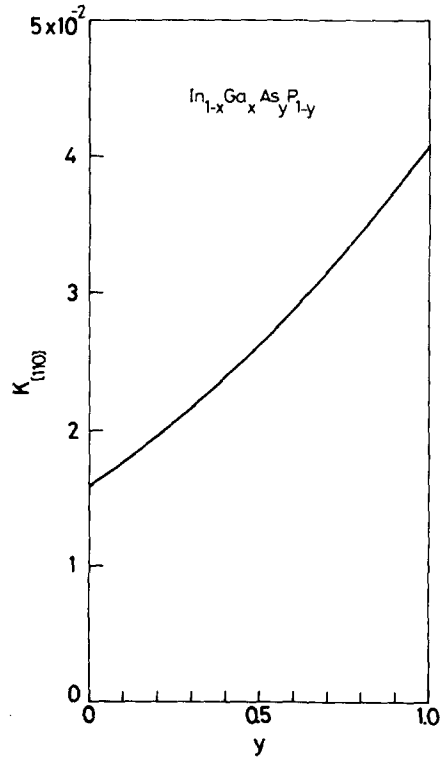


FIG. 28. Electromechanical coupling constant $K_{[110]}$ as a function of the $y$-composition parameter for $In_{1-x}Ga_xAs_yP_{1-y}$ lattice-matched to InP.

completely understood at present.

It is well known[48] that injected ultrasonic waves can be amplified in piezoelectric semiconductors by the application of a sufficiently high electric field because of the strong interaction with mobile charge carriers. Domains of intense acoustic flux, showing a broad band of frequencies in the low-GHz range, can also be produced in semiconductors, such as GaAs[49] and GaSb,[50] by acoustoelectric amplification of phonons from the thermal equilibrium spectrum. The gain of such acoustoelectric interactions can be explained in terms of the material parameter, $K^2$, called to as the electromechanical coupling constant.[48] The coupling constant $K^2$ is a crystal-direction dependent quantity. The maximum coupling of the transverse waves is along [110] direction for the zincblende-type crystal, which is the reason why the majority of experiments have been carried out with crystals cut in this direction.[48,51] In this case, the constant can be written as

$$K^2_{[110]} = \frac{e_{14}^2}{\epsilon_s C_{44}}, \tag{28}$$

where $e_{14}$ is the piezoelectric constant, $\epsilon_s$ the dielectric constant, and $C_{44}$ is the elastic stiffness constant. Figure 28 shows the coupling contant $K_{[110]}$ calculated from Eq. (28) versus $y$ for $In_{1-x}Ga_xAs_yP_{1-y}$ lattice-matched to InP.

### J. Deformation potential

It has been shown that the lattice mobility of holes in III-V compounds is limited primarily by acoustic and nonpolar optical mode scattering.[39] The strength of these scattering mechanisms is determined essentially by the valence-band deformation potentials, namely $a$, $b$, and $d$ (Pikus-Bir's notation).[52] Fundamental optical properties, e.g., piezobirefringence and Raman (Brillouin) scattering,[53] are also strongly affected by these potentials. The purpose of this subsection is to estimate values of the deformation potentials for $In_{1-x}Ga_xAs_yP_{1-y}$ quaternaries.

Although the shear deformation potentials "$b$" and "$d$" have been measured for many materials, it is difficult to obtain values for the hydrostatic-like potential "$a$" since most experiments measure changes in energy gaps and their related effects rather than absolute shifts of the band edges. However, Lawaetz[54,55] has proposed a theoretical expression based on the dielectric band theory of Phillips[38] which allows "$a$" to be estimated with reasonable accuracy. His theory leads to the following expression for a[55]:

$$a = -0.4\frac{E_{vh}^2}{E_v} - 0.7\frac{C^2}{E_v}. \tag{29}$$

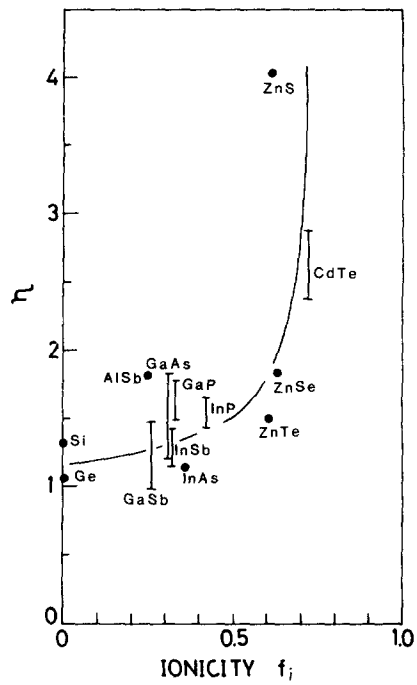


FIG. 30. Plots of $\eta = d/\sqrt{3}b$ versus Phillips's ionicity $f_i$ for all the measured covalent and zincblende-type materials.

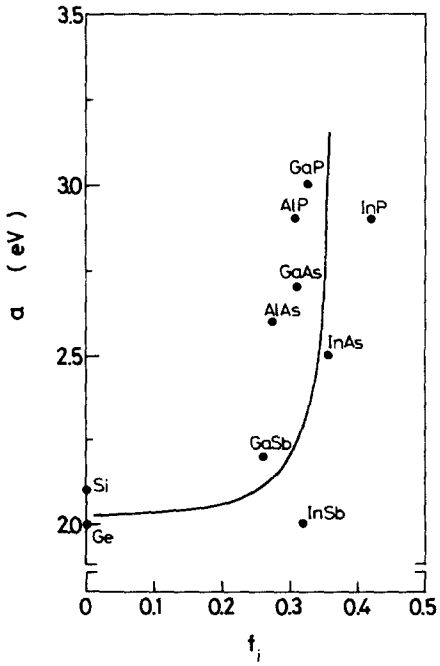


FIG. 29. Plots of "$a$" versus Phillips's ionicity $f_i$ for some of the covalent and III-V materials.

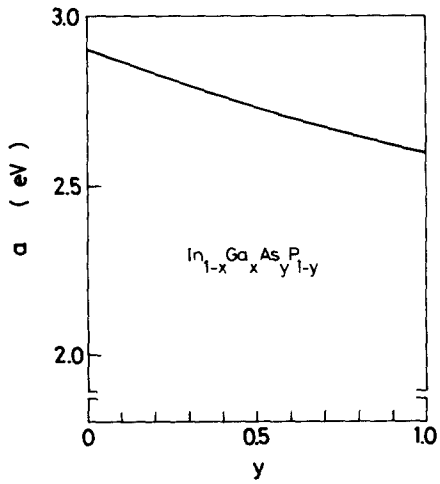


FIG. 31. Deformation potential "$a$" as a function of the $y$-composition parameter for $In_{1-x}Ga_xAs_yP_{1-y}$ lattice-matched to InP.

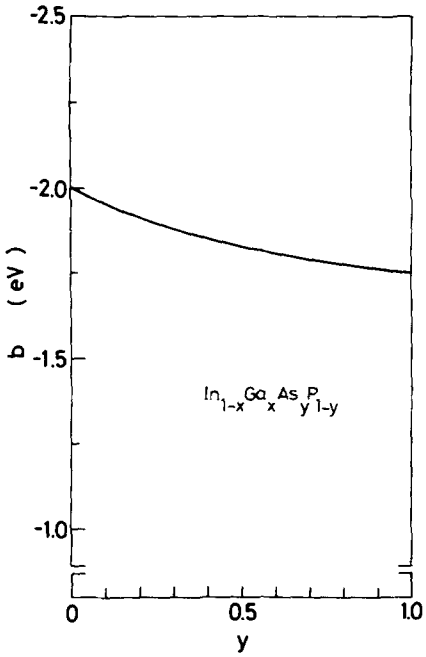


FIG. 32. Deformation potential "$b$" as a function of the $y$-composition parameter for $In_{1-x}Ga_xAs_yP_{1-y}$ lattice-matched to InP.

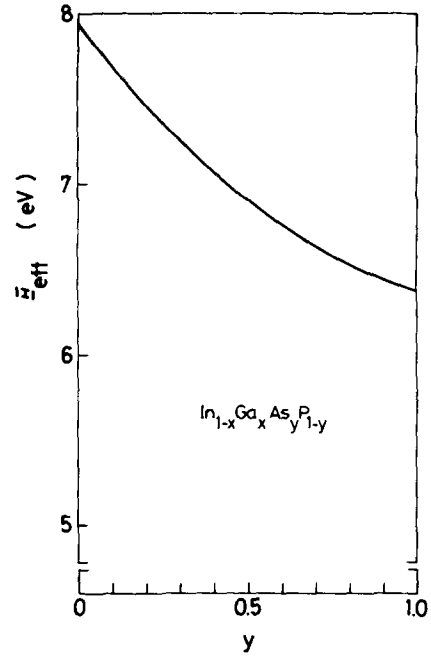


FIG. 34. Effective acoustic deformation potential $\Xi_{eff}$ as a function of the $y$-composition parameter for $In_{1-x}Ga_xAs_yP_{1-y}$ lattice-matched to InP.

In Eq. (29), $a$, $E_v$, $E_{vh}$, and $C$ are in eV (in the notation of Ref. 55). The parameter $C$ is Phillips's ionic energy gap. Equation (29) recalls existence of any relation between the quantity $a$ and Phillips's ionicity $f_i$. The plots of "$a$" calculated from Eq. (29)[39,55] versus $f_i$ for some of the covalent and III-V materials are shown in Fig. 29. We find from the figure that there is an increase in $a$ with increasing $f_i$. In Fig. 30, we have also plotted the values of $\eta = d/\sqrt{3}b$, that is the ratio of the splitting for a shear strain along [111] to the splitting for a shear strain of the same magnitude along [100], for all the measured covalent and zincblende-type materials. One can also find an increase in $\eta$ with increasing $f_i$, similar to the case for "$a$". Such trends can be well interpreted by a point-ion model proposed by Gavini and Cardona.[56,57]

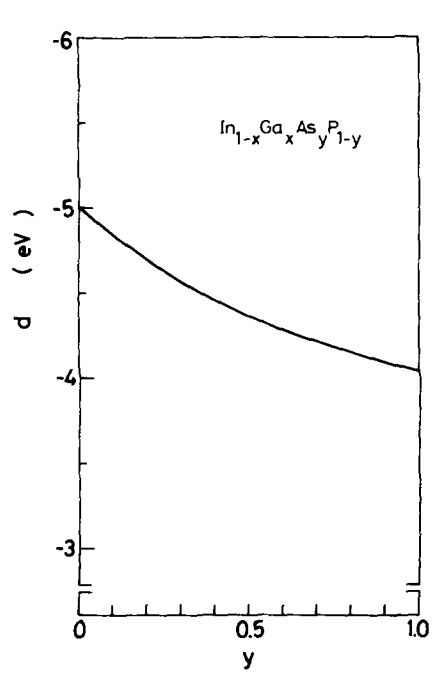


FIG. 33. Deformation potential "$d$" as a function of the $y$-composition parameter for $In_{1-x}Ga_xAs_yP_{1-y}$ lattice-matched to InP.

The interpolated values of $a$, $b$, and $d$, as a function of the $y$-component parameter, for $In_{1-x}Ga_xAs_yP_{1-y}$ lattice-matched to InP are shown in Figs. 31–33, respectively. As can be seen, these values increase with decreasing $y$ (or with increasing Phillips's ionicity: see Fig. 20) which agree well with the general trends obtained in Figs. 29 and 30.

There are various studies relating the stress effects on lasing characteristics of GaAlAs/GaAs laser diodes.[58] For $In_{1-x}Ga_xAs_yP_{1-y}$, the deformation potentials associated with [100] and [111] stresses, respectively, are $b = -1.81$ and $d = -4.27$ eV [$y \simeq 0.6$, $\lambda_0 \simeq 1.3$ $\mu$m] and $b = -1.76$ and $d = -4.08$ eV [$y \simeq 0.9$; $\lambda_0 \simeq 1.55$ $\mu$m]. The corresponding laser-energy shifts (or energy-gap shifts) $\Delta E$ with the applied stress $X$ are given by the relation: $\Delta E = b(S_{11} - S_{12})X$ eV/bar for [100] stress and $\Delta E = (d/2\sqrt{3})S_{44}X$ eV/bar for [111] stress [$S_{ij}$: elastic compliance constant].

Lawaetz[54] has determined an effective acoustic-mode deformation potential, $\Xi_{eff}$, appropriate to low-field transport in $p$-type materials with Ge-like (zincblende) valence bands. This parameter is given by

$$\Xi_{eff}^2 = a^2 + \frac{C_l}{C_t}\left(b^2 + \frac{1}{2}d^2\right), \tag{30}$$

where $C_l$ and $C_t$ are spherically averaged elastic coefficients given by

$$C_l = \tfrac{1}{5}(3C_{11} + 2C_{12} + 4C_{44}), \tag{31a}$$

$$C_t = \tfrac{1}{5}(C_{11} - C_{12} + 3C_{44}). \tag{31b}$$

Figure 34 shows the values of $\Xi_{eff}$ calculated from Eq. (30)

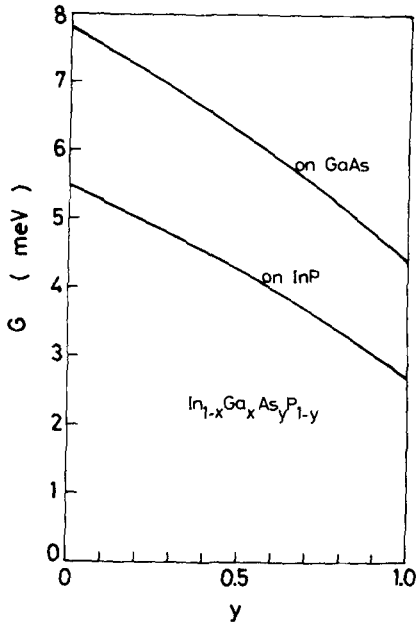


FIG. 35. Exciton Rydberg energy $G$ as a function of the $y$-composition parameter for $In_{1-x}Ga_xAs_yP_{1-y}$ lattice-matched to InP and GaAs.

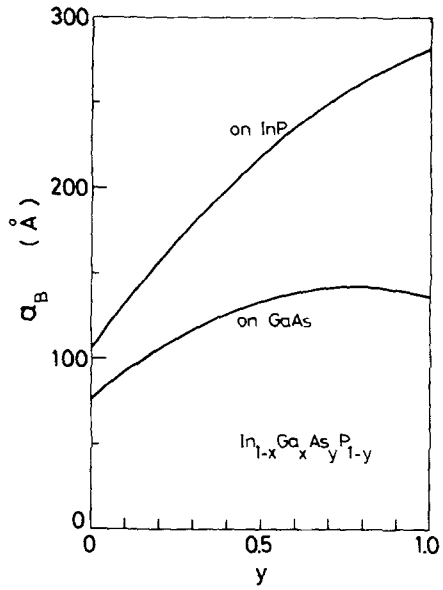


FIG. 36. Exciton Bohr radius $a_B$ vs $y$ for $In_{1-x}Ga_xAs_yP_{1-y}$ lattice-matched to InP and GaAs.

versus $y$ for $In_{1-x}Ga_xAs_yP_{1-y}$ lattice-matched to InP. The numerical values used are taken from Fig. 22 for $C_{ij}$, from Fig. 31 for $a$, from Fig. 32 for $b$, and from Fig. 33 for $d$. The values of $\Xi_{\text{eff}}$ decrease monotonically with increasing the $y$-composition proportion.

### K. Excitonic effect

The phenomenon of excitons in crystals has been a subject of considerable interest for many years and has been summarized in general by Knox,[59] and in particular with respect to the group III-V compounds by Dimmock.[60] Exciton transitions play a momentous role in the fundamental optical processes in solids, such as emission and absorption of photons. The Coulomb interaction is always present between the electrons and holes. The exciton state and its behaviors are known to be characterized by the exciton Rydberg energy $G$ [in eV]:

$$G = \frac{\mu e^4}{2\hbar^2 \epsilon_s^2} = 13.6\left(\frac{\mu}{m_0}\right)\frac{1}{\epsilon_s^2}, \tag{32}$$

where $\mu$ is the reduced exciton mass, $e$ the electron charge, and $\epsilon_s$ is the dielectric constant. The exciton Bohr radius $a_B$ [in Å] is now given by

$$a_B = \frac{\hbar^2 \epsilon_s}{\mu e^2} = 0.53\epsilon_s\left(\frac{m_0}{\mu}\right). \tag{33}$$

Figure 35 shows the calculated values of $G$ as a function of the $y$-composition proportion for $In_{1-x}Ga_xAs_yP_{1-y}$ lattice-matched to InP and GaAs. The values of $a_B$ are also shown in Fig. 36. The material parameters used in the calculations were taken from Figs. 12, 13, and 18. Since we used the linear interpolation scheme of Eq. (3), the values of $G$ and $a_B$ in Figs. 35 and 36 were not properly taken into account the effects of alloy disorder. The exciton spectrum is known to be strongly affected by damping, i.e., a lifetime broadening.[53] The damping effect should be influenced by the lattice disorder, as well as the thermal vibrations and lattice defects. In fact, Goede *et al.*[61] have observed disorder-induced broadening of the exciton line in the II-VI mixed crystals. Henning and Strehlow[62] have, however, recently shown theoretically that this contribution is negligibly small in the case of the III-V mixed crystals.

## IV. CONCLUSION

$In_{1-x}Ga_xAs_yP_{1-y}$ quaternary system has attracted great interest because it can be grown epitaxially on InP substrate without lattice mismatch over a wide range of compositions covering a broad range of band gaps (0.75–1.35 eV), and thus complex multilayered devices can be produced. A number of important semiconductor properties of $In_{1-x}Ga_xAs_yP_{1-y}$ for their analysis require quite detailed knowledge of material parameters, but it is at present rather difficult to obtain the most reliable values from the literature reported. Various models for calculation of physical parameters in compound alloys are discussed, and the results for $In_{1-x}Ga_xAs_yP_{1-y}$ quaternaries are presented. A linear interpolation has been used for want of any more detailed experimental data, and that the accuracy of the interpolated values are probably estimates only. It is found that the present model provides generally acceptable parameters, in good agreement with the existing experimental data. A detailed discussion is also given on the acceptability of the interpolated parameters in connection with the solid-state physics. Key properties of the material parameters for a variety of $In_{1-x}Ga_xAs_yP_{1-y}$ device applications are also discussed.


## ACKNOWLEDGMENTS

The author wished to thank Y. Katoh, Y. Suemune, T. Ikegami, G. Iwane, and H. Kawaguchi for their encouragement and kind advice throughout this work.

## APPENDIX A: Key properties of $In_{1-x}Ga_xAs_yP_{1-y}$/ ZnSe relevant to device design

The properties of heterojunctions that permit much lower threshold current densities than homostructure lasers can best be illustrated with the double heterostructure. The most important factors in heterostructure lasers are the energy gap and refractive index. ZnSe has a direct band gap of 2.68 eV (at room temperature), and is thought to be a very promising material for blue and green electroluminescent devices. The $In_{1-x}Ga_xAs_yP_{1-y}$/ZnSe heterostructure, thus, provides the band-gap difference larger than 0.80 eV (see Fig. 6), which is sufficient to confine the injected carriers.

By using the interpolation method, we can calculate the refractive indices of the $In_{1-x}Ga_xAs_yP_{1-y}$ quaternaries. The real part of the dielectric constant $\epsilon_1(\omega)$ in the zincblende-type material below the band edge can be written as

$$\epsilon_1(\omega) = A\{f(\chi) + \tfrac{1}{2}[E_0/(E_0+\Delta_0)]^{3/2} f(\chi_{so})\} + B, \quad \text{(A1)}$$

with

$$f(\chi) = \chi^{-2}[2 - (1+\chi)^{1/2} - (1-\chi)^{1/2}], \quad \text{(A2)}$$

$$\chi = \hbar\omega/E_0, \quad \text{(A3)}$$

$$\chi_{so} = \hbar\omega/(E_0+\Delta_0). \quad \text{(Ref. 63)} \quad \text{(A4)}$$

In Eqs. (A1)–(A4), $A$ and $B$ are constants and $\hbar\omega$ is the photon energy. The constants $A$ and $B$, determined by fitting Eq. (A1) with the data of binaries, are $A = 9.29$ and $B = 7.86$ for GaAs, $A = 22.25$ and $B = 0.90$ for GaP, $A = 4.36$ and $B = 10.52$ for InAs, and $A = 8.40$ and $B = 6.60$ for InP. Introducing the interpolated values of $A$ and $B$, and $E_0$ and $\Delta_0$ (see Fig. 7) into Eq. (A1), one obtains the value of $\epsilon_1(\omega)$ for $In_{1-x}Ga_xAs_yP_{1-y}$ lattice-matched to ZnSe. The values of $\epsilon_1(\omega)$ for ZnSe, on the other hand, are taken in the literature.[64] Since the imaginary part of the dielectric constant may be taken as zero in the region of the lowest-direct gap, one obtains the frequency-dependent refractive index $n(\omega)$ in the relation:

$$n(\omega) \simeq \epsilon_1(\omega)^{1/2}. \quad \text{(A5)}$$

The calculated refractive-index steps between ZnSe and $In_{1-x}Ga_xAs_yP_{1-y}$ lattice-matched to ZnSe as a function of the photon energy are shown in Fig. A1. As can be seen from the figure, this system provides a large refractive-index step within a whole range of the $y$-composition for the light confinement in an active region.

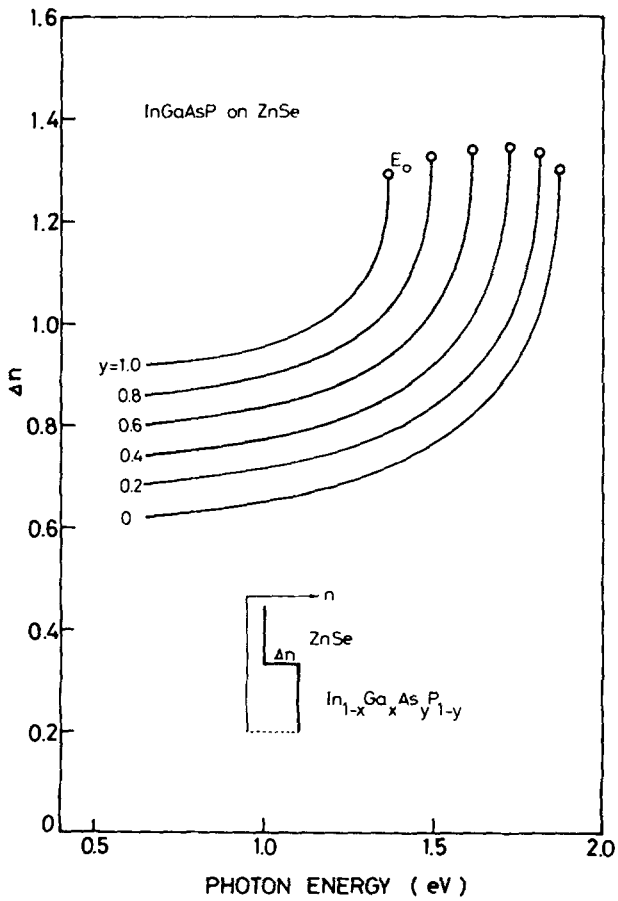


FIG. A1. Refractive-index steps between ZnSe and $In_{1-x}Ga_xAs_yP_{1-y}$ lattice-matched to ZnSe as a function of the photon energy.

## APPENDIX B: Optical transitions at the region near the $\Gamma$-point valence bands

The zincblende-type crystal has a $T_d$ point-group structure. It is known that at $\vec{k} = 0$, the conduction band has $\Gamma_6$ symmetry and the $A$ (heavy-hole), $B$ (light-hole), and $C$ (split-off) valence bands have $\Gamma_8$, $\Gamma_8$, and $\Gamma_7$ symmetries, respectively. The light polarization vector $\vec{E} \perp (\vec{x}, \vec{y}, \vec{z})$ of the point group $T_d$ belongs to $\Gamma_5$ symmetry. The optical transitions between the valence bands can be given by the direct products

$$\Gamma_7 \rightarrow \Gamma_8 (C \rightarrow A): \Gamma_7 \times \Gamma_8 = \Gamma_3 + \Gamma_4 + \Gamma_5, \quad \text{(B1)}$$

$$\Gamma_7 \rightarrow \Gamma_8 (C \rightarrow B): \Gamma_7 \times \Gamma_8 = \Gamma_3 + \Gamma_4 + \Gamma_5. \quad \text{(B2)}$$

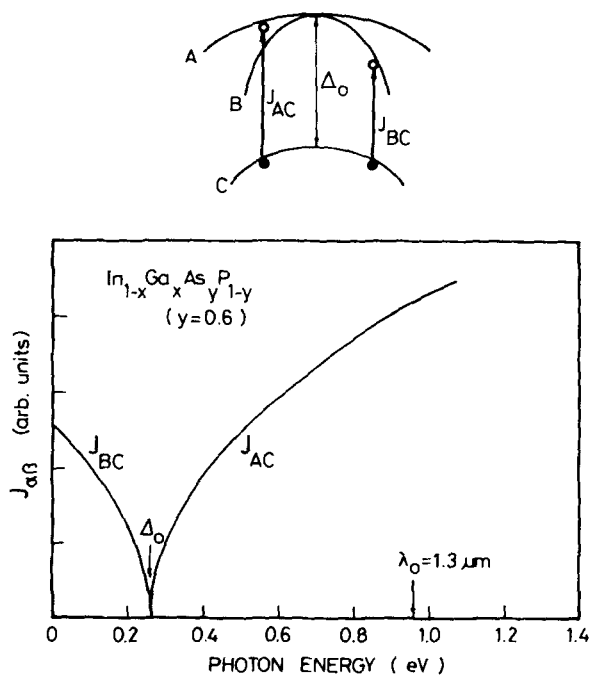


FIG. A2. Joint density of states $J_{\alpha\beta}$ against energy for different critical points in the valence bands.

It is clear from Eqs. (B1) and (B2) that the transitions contain the representation of $\Gamma_5$ symmetry. It means that the optical transition between the $C$ and $A$ (or $B$) valence bands is possible.

The joint density of states function $J_{\alpha\beta}(\omega)$ measures the product density of full and empty states of equal energy difference. This quantity is mainly determining the interband contribution to $\epsilon_2(\omega)$, and thus to the optical constants of solids. According to different combinations of the sign of

$$(1/\mu_i = 1/m_{\alpha e} + 1/m_{\beta h})_{\vec{k}=\vec{k}_0}, \quad (i = x,y,z), \tag{B3}$$

one has to distinguish between four types of critical points, $M_0$, $M_1$, $M_2$, and $M_3$ (van Hove's singularities). The states $\alpha$ and $\beta$ mean empty (electron) and full (hole) bands, respectively. The effective mass, e.g., in the $\alpha$ band, has the relation

$$m_{\alpha e} = -m_{\alpha h} \tag{B4}$$

between the electron mass $m_{\alpha e}$ and hole mass $m_{\alpha h}$. The type of singularities in the case of the $\Gamma$-point valence bands can be determined by inserting the values of effective masses (Fig. 13) into Eq. (B3). The results show that $J_{AC}$ ($C \rightarrow A$) and $J_{BC}$ ($C \rightarrow B$) are represented by $M_0$-type and $M_3$-type critical points, respectively. The $M_0$-type ($M_3$-type) critical point is realized by having all $\mu_i > 0$ ($\mu_i < 0$). The $\omega$-dependent states functions are, thus, written as

$$J_{CA}(\omega)\begin{cases} = C_0(\hbar\omega - \Delta_0)^{1/2} & , (\hbar\omega > \Delta_0) \\ = 0 & , (\hbar\omega < \Delta_0) \end{cases} \tag{B5}$$

$$J_{CB}(\omega)\begin{cases} = 0 & , (\hbar\omega > \Delta_0) \\ = C_1(\Delta_0 - \hbar\omega)^{1/2} & , (\hbar\omega < \Delta_0) \end{cases} \tag{B6}$$

Figure A2 shows qualitatively the form of $J_{\alpha\beta}$ for these two cases. The energy scale corresponds to that for $In_{1-x}Ga_xAs_yP_{1-y}$ ($y \simeq 0.6$, $\lambda_0 \simeq 1.3$ $\mu$m). Note that the strength of optical absorption is proportional to $J_{\alpha\beta}$. The figure clearly suggests the possibility of new optical absorption in the $In_{1-x}Ga_xAs_yP_{1-y}$/InP lasers due to electronic transitions between the $\Gamma_7(C)$ and $\Gamma_8(A)$ valence bands, as also pointed out by Suematsu and co-workers [see Ref. 35].


[1]T. P. Pearsall, IEEE J. Quantum Electron. **QE-16**, 709 (1980).
[2]P. A. Houston, J. Mater. Sci. **16**, 2935 (1981).
[3]R. E. Nahory, M. A. Pollack, W. D. Johnston, Jr. and R. L. Barns, Appl. Phys. Lett. **33**, 659 (1978).
[4]P. M. Laufer, F. H. Pollak, R. E. Nahory, and M. A. Pollack, Solid State Commun. **36**, 419 (1980).
[5]E. H. Perea, E. E. Mendez, and C. G. Fonstad, Appl. Phys. Lett. **36**, 978 (1980).
[6]Y. Yamazoe, T. Nishino, and Y. Hamakawa, IEEE J. Quantum Electron. **QE-17**, 139 (1981).
[7]R. Madelon and M. Dore, Solid State Commun. **39**, 639 (1981).
[8]G. H. Olsen, T. Z. Zamerowski, R. T. Smith, and E. P. Bertin, J. Electron. Mater. **9**, 977 (1980).
[9]R. L. Moon, G. A. Antypas, and L. W. James, J. Electron. Mater. **3**, 635 (1974).
[10]B. Abeles, Phys. Rev. **131**, 1906 (1963).
[11]J. A. van Vechten and T. K. Bergstresser, Phys. Rev. B **1**, 3351 (1970).
[12]T. H. Glisson, J. R. Hauser, M. A. Littlejohn, and C. J. Williams, J. Electron. Mater. **7**, 1 (1978).
[13]R. Bisaro, P. Merenda, and T. P. Pearsall, Appl. Phys. Lett. **34**, 100 (1979).
[14]M. E. Stranmanis and J. P. Krumme, J. Electrochem. Soc. **114**, 640 (1967).
[15]H. P. Singh and B. Dayal, Phys. Status Solidi **23**, K93 (1967).
[16]H. C. Casey, Jr. and M. B. Panish, in *Heterostructure Lasers, Part B* (Academic, New York, 1978).
[17]T. Yuasa, *Pap. Tech. Group Meet. Optics & Quantum Electron. of IECE Japan*, **OQE81-17** (1981), (in Japanese).
[18]S. Arai, Y. Suematsu, and Y. Itaya, IEEE J. Quantum Electron. **QE-16**, 197 (1980).
[19]D. L. Rode, Phys. Rev. B **2**, 1012 (1970).
[20]D. L. Rode, Phys. Rev. B **3**, 3287 (1971).
[21]Y. Takeda, M. A. Littlejohn, and J. R. Hauser, Appl. Phys. Lett. **39**, 620 (1981).
[22]A. K. Saxena, Phys. Rev. B **24**, 3295 (1981).
[23]Y. Takeda, M. A. Littlejohn, J. A. Hutchby, and R. J. Trew, Electron. Lett. **17**, 686 (1981), and references therein.
[24]J. B. Restorff, B. Houston, J. R. Burke, and R. E. Hayes, Appl. Phys. Lett. **32**, 189 (1978).
[25]R. J. Nicholas, J. C. Portal, C. Houlberg, P. Perrier, and T. P. Pearsall, Appl. Phys. Lett. **34**, 492 (1979).
[26]H. Brendecke, H. L. Stormer, and R. J. Nelson, Appl. Phys. Lett. **35**, 772 (1979).
[27]R. J. Nicholas, S. J. Sessions, and J. C. Portal, Appl. Phys. Lett. **37**, 178 (1980).
[28]J. B. Restorff, B. Houston, R. S. Allgaier, M. A. Littlejohn, and S. B. Phatak, J. Appl. Phys. **51**, 2277 (1980).
[29]E. H. Perea, E. Mendez, and C. G. Fonstad, J. Electron. Mater. **9**, 459 (1980).
[30]L. M. Roth, B. Lax, and S. Zwerdling, Phys. Rev. **114**, 90 (1959).
[31]R. J. Nicholas, J. C. Portal, C. Houlbert, P. Perrier, and T. P. Pearsall, Appl. Phys. Lett. **34**, 429 (1979).
[32]R. J. Nicholas, R. A. Stradling, and J. C. Ramage, J. Phys. C **12**, 1641 (1979).
[33]P. Lawaetz, Phys. Rev. B **4**, 3460 (1971).
[34]C. Hermann and T. P. Pearsall, Appl. Phys. Lett. **38**, 450 (1981).
[35]M. Asada, A. R. Adams, K. E. Stubkjaer, Y. Suematsu, Y. Itaya, and S. Arai, IEEE J. Quantum Electron. **QE-17**, 611 (1981).
[36]See, for example, F. Abeles, in *Optical Properites of Solids* (North-Holland, Amsterdam, 1972).
[37]See, for example, S. M. Sze, *Physics of Semiconductor Devices* (Wiley, New York, 1981).
[38]J. C. Phillips, *Bonds and Bands in Semiconductors* (Academic, New York, 1973).
[39]R. K. Willardson and A. C. Beer, in *Semiconductors and Semimetals* (Academic, New York, 1975), Vol. 10.
[40]J. T. Devreese, *Polarons in Ionic Crystals and Polar Semiconductors* (North-Holland, Amsterdam, 1972).
[41]R. J. Nicholas, R. A. Stradling, J. C. Portal, and S. Askenazy, J. Phys. C **12**, 1653 (1979).
[42]J. F. Nye, *Physical Properties of Crystals* (Clarendon, Oxford, 1972).
[43]B. W. Hakki, A. Jayaraman, and C. K. Kim, J. Appl. Phys. **41**, 5291 (1970).
[44]D. L. Rode, Phys. Rev. B **2**, 4036 (1970).
[45]G. Arlt and P. Quadflieg, Phys. Status Solidi **25**, 323 (1968).
[46]J. C. Phillips and J. A. van Vechten, Phys. Rev. Lett. **23**, 1115 (1969).
[47]M. Miura, H. Murata, Y. Shiro, and K. Iishi, J. Phys. Chem. Solids **42**, 931 (1981).
[48]N. I. Meyer and M. H. Jörgensen, *Advances in Solid State Physics*, edited by O. Madelung (Pergamon, Vieweg, 1970), p. 21.
[49]D. L. Spears, Phys. Rev. B **2**, 1931 (1970).
[50]P. O. Sliva and R. Bray, Phys. Rev. Lett. **14**, 372 (1965).
[51]R. Klein, Solid State Commun. **7**, 917 (1969).
[52]G. E. Pikus and G. L. Bir, Sov. Phys.-Solid State **1**, 136 (1959).
[53]S. Adachi and C. Hamaguchi, Phys. Rev. B **19**, 938 (1979).
[54]P. Lawaetz, Phys. Rev. **166**, 763 (1968); **174**, 867 (1968); **183** 730 (1969).
[55]J. D. Wiley, Solid State Commun. **8**, 1865 (1970).
[56]A. Gavini and M. Cardona, Phys. Rev. **177**, 1351 (1969).
[57]A. Gavini and M. Cardona, Phys. Rev. B **1**, 672 (1970).
[58]H. Kressel and J. K. Butler, *Semiconductor Lasers and Heterojunction LEDs* (Academic, New York, 1977).
[59]R. S. Knox, *Theory of Excitons* (Academic, New York, 1963).
[60]J. O. Dimmock, *Semiconductors and Semimetals*, edited by R. K. Willardson and A. C. Beer (Academic, New York, 1967), Vol. 3.
[61]O. Goede, D. Henning, and L. John, Phys. Status Solidi (b) **96**, 671 (1979).
[62]D. Henning and R. Strehlow, Phys. Status Solidi (b) **107**, 283 (1981).
[63]S. Adachi, J. Appl. Phys. **53**, 5863 (1982).
[64]D. T. F. Marple, J. Appl. Phys. **35**, 539 (1964).